PAPER

Core–shell fibrous threads loaded with VEGF plasmid polyplexes for sustained, threshold-guided gene delivery

Biomedical Materials

PAPER

RECEIVED
13 February 2026

REVISED
14 June 2026

ACCEPTED FOR PUBLICATION
29 June 2026

PUBLISHED
20 July 2026

Core–shell fibrous threads loaded with VEGF plasmid polyplexes for sustained, threshold-guided gene delivery

Farzaneh Ghasemkhah[1,*], Masoud Latifi[2,*], Afra Hadjizadeh[3], Mohammad Ali Shokrgozar[4], Fatemeh Radmanesh[5,6], Hamid Sadeghi Abandansari[6,7], Mahdi Hesaraki[8] and Shahram Azari[4]

[1] Department of Materials and Textile Engineering, Faculty of Engineering, Razi University, Kermanshah, Iran
[2] Textile Engineering Department, Textile Excellence & Research Centers, Amirkabir University of Technology, Tehran, Iran
[3] Biomedical Engineering Department, Amirkabir University of Technology, Tehran, Iran
[4] National Cell Bank of Iran, Pasteur Institute of Iran, Tehran, Iran
[5] Uro-Oncology Research Center, Tehran University of Medical Sciences, Tehran, Iran
[6] Department of Cell Engineering, Cell Science Research Center, Royan Institute for Stem Cell Biology and Technology, ACECR, Tehran, Iran
[7] Department of Stem Cells and Developmental Biology, Faculty of Sciences and Advanced Technologies in Biology, University of Science and Culture, Tehran, Iran
[8] Department of Animal Sciences and Marine Biology, Faculty of Life Sciences and Biotechnology, Shahid Beheshti University, Tehran, Iran
[*] Authors to whom any correspondence should be addressed.

E-mail: f.ghasemkhah@razi.ac.ir and Latifi@aut.ac.ir

Keywords: angiogenesis, coaxial electrospinning, core-shell fibers, deoxycholic acid-modified PEI, fibrous thread, non-viral gene delivery, VEGF delivery

Abstract

Precise regulation of vascular endothelial growth factor (VEGF) delivery is essential for angiogenesis-oriented tissue engineering, because excessive or poorly controlled VEGF exposure may lead to abnormal and immature vascular structures. In this study, aligned core–shell fibrous threads loaded with deoxycholic acid-modified branched polyethylenimine/plasmid encoding VEGF ($bPEI_{1.8}$-DA/plasmids encoding vascular endothelial growth factor (pVEGF)) polyplexes were developed as a scaffold-mediated platform for sustained VEGF gene delivery. The polymer/plasmid DNA weight ratio was first optimized in human umbilical vein endothelial cells (HUVECs), and a ratio of 2 was selected based on reporter-gene expression and cytocompatibility. The pVEGF polyplexes were then incorporated into the aqueous core of gelatin/poly(ε-caprolactone) (70:30) fibers using modified coaxial electrospinning equipped with a rotating disk collector. Electron and fluorescence microscopy confirmed the formation of bead-free aligned fibers with a core–shell architecture and successful polyplex incorporation. The aligned fibers were twisted into cohesive fibrous threads with an average diameter of approximately 148 μm. Genipin crosslinking preserved the fibrous morphology, improved scaffold stability, and increased Young's modulus from 37.13 to 49.81 cN/Tex while reducing extensibility. *In vitro* release studies showed that the core–shell structure, crosslinking, and compact thread architecture reduced the initial burst release and prolonged polyplex delivery over 33 d. The initial polyplex release from crosslinked threads was 16.59%, approximately 35% lower than that from crosslinked webs, and the released polyplex amount remained below the 100 ng threshold level for up to 16 d. Released polyplexes retained reporter-gene expression capability, and enzyme-linked immunosorbent assay confirmed prolonged VEGF secretion by HUVECs. The scaffolds also supported cell adhesion and

metabolic activity. These findings indicate that aligned core–shell fibrous threads can provide sustained plasmid polyplex availability, prolong downstream VEGF secretion, and serve as a promising platform for localized angiogenic gene delivery, particularly in applications requiring directional fibrous architecture and localized vector delivery.

1. Introduction

Vascularization remains one of the most significant challenges for the success of engineered tissue constructs designed to repair or replace damaged tissues [1–3]. Extracellular matrix (ECM)-mimicking scaffolds with appropriate architectural configurations [4, 5] and localized delivery of angiogenic growth factors (GFs) [6, 7] are promising strategies for improving vascularization. Polymeric scaffolds play an important role in therapeutic angiogenesis by providing a temporary porous architectural guide that supports endothelial cell adhesion [8]. Since angiogenesis depends strongly on the dose and duration of angiogenic stimulation, sustained and controlled delivery of GFs is essential for effective and organized blood vessel formation [9, 10]. Therefore, combining polymeric scaffolds with angiogenic agents can help regulate GF release according to target tissue requirements through coordinated optimization of scaffold architecture and the type and concentration of the delivered agent [11–13].

Vascular endothelial growth factor (VEGF) is one of the most important regulators of angiogenesis and plays a key role in basement membrane degradation, endothelial cell proliferation, sprouting, and new vessel formation [14, 15]. However, the angiogenic outcome of VEGF strongly depends on its local concentration and exposure duration. Uncontrolled or excessive VEGF delivery can induce abnormal, immature, and leaky vascular structures and may increase the risk of hemangioma-like vessel formation [16–18]. Although co-delivery of multiple GFs has been proposed to improve vascular maturation [19–21], previous studies have shown that long-term, low-level, continuous VEGF delivery can promote more organized angiogenesis when local VEGF levels are maintained below a critical threshold [16]. Therefore, a delivery platform that can maintain local VEGF concentrations at low, steady levels over a prolonged period is highly desirable for regenerative medicine applications.

Direct delivery of VEGF protein has been widely explored; however, this approach is limited by the short half-life of GFs, possible loss of bioactivity during scaffold fabrication, high cost, and rapid diffusion from the implantation site. VEGF gene delivery provides an alternative strategy by enabling transfected cells to produce VEGF locally and continuously over time [22–27]. The success of this approach strongly depends on the selection of an appropriate gene delivery vector. Non-viral polymeric vectors are particularly attractive because of their ease of preparation, structural tunability, and lower immunogenicity compared with viral vectors [28–30]. Among these systems, polyethylenimine (PEI)-based vectors have been widely investigated because of their strong nucleic acid condensation ability [31–34]. High-molecular-weight branched PEI, such as bPE_{I25}, generally shows high transfection efficiency but is associated with considerable cytotoxicity, whereas low-molecular-weight $bPEI_{1.8}$ offers improved cytocompatibility but limited gene delivery efficiency. Therefore, chemical modification of $bPEI_{1.8}$ has been explored to improve its transfection performance while preserving its relatively favorable safety profile [35–43]. Deoxycholic acid-modified $bPEI_{1.8}$ has previously been developed and evaluated as an amphiphilic non-viral vector with improved nucleic acid complexation and gene delivery capability in human umbilical vein endothelial cells (HUVECs) [42–46]. Based on these previous findings, $bPEI_{1.8}$-DA was selected in the present study as the non-viral vector for plasmids encoding vascular endothelial growth factor (pVEGF) delivery.

Incorporating angiogenic gene vectors into polymeric scaffolds is a promising strategy for localized gene delivery because it can prolong vector availability at the target site, reduce off-target distribution, and improve the safety of gene-based angiogenic stimulation [47–49]. Conventional electrospun nanofibers are attractive for this purpose because of their ECM-like architecture and high surface area [50–52]; however, they may exhibit rapid initial release of gene-vector complexes [53]. Core–shell electrospun structures can address this limitation by placing the gene-vector cargo within the core and using the shell layer to regulate diffusion and protect sensitive genetic materials during delivery [54–58]. Hereupon, coaxial electrospinning is considered a remarkable breakthrough in the release of susceptible agents [59, 60]. In our previous study, a gelatin/PCL core–shell electrospinning platform was developed to control the release of model proteins from the aqueous core [61]. Building on this platform, the present study extends the core–shell design from protein release to pVEGF polyplex delivery. While most electrospun gene delivery scaffolds have been developed as two-dimensional non-woven webs, aligned fibrous

threads may provide additional advantages, including directional architecture, reduced burst release, and potential integration into three-dimensional tissue engineering systems.

In this study, we introduce a transition from conventional two-dimensional non-woven coaxial webs to aligned core–shell fibrous threads for scaffold-mediated VEGF gene delivery. These threads are intended for future integration with three-dimensional co-culture platforms, where they may provide directional guidance together with localized and sustained delivery of angiogenic gene vectors. Accordingly, core–shell fibrous threads loaded with deoxycholic acid-modified branched PEI/plasmid encoding VEGF ($bPEI_{1.8}$-DA/pVEGF) polyplexes were developed for sustained, threshold-guided VEGF gene delivery. The $bPEI_{1.8}$-DA vector was selected based on its previously reported ability to form stable nucleic acid nanocomplexes and improve gene delivery performance in HUVECs [62]. Before scaffold loading, the polymer/plasmid ratio was optimized in HUVECs to identify a formulation with a suitable balance between reporter-gene expression and cytocompatibility. Based on our previous core–shell electrospinning platform, a gelatin/PCL (70:30) blend was used as the shell layer, while the pVEGF polyplexes were incorporated into the aqueous core by coaxial electrospinning. A rotating disk collector was then used to obtain aligned fibrous bundles suitable for thread fabrication. The developed scaffolds were evaluated in terms of morphology, core–shell structure, mechanical properties, release behavior, cytocompatibility, HUVEC adhesion, reporter-gene expression capability after release, and VEGF secretion by ELISA. The overall aim was to develop a fibrous thread-based platform capable of providing sustained pVEGF polyplex delivery while maintaining VEGF expression within a controlled and biologically relevant range.

2. Materials and methods

2.1. Materials

Gelatin type A from porcine skin and poly(ε-caprolactone) (PCL, Mw = 80 000 g mol^{-1}) were purchased from Sigma-Aldrich. Fluorescein isothiocyanate (FITC) and rhodamine B isothiocyanate (RBITC) were also obtained from Sigma-Aldrich for fluorescence labeling. 2,2,2-Trifluorethanol (TFE, purity ⩾99%) and bovine serum albumin (BSA, purity ⩾98%) were purchased from Merck. Genipin, used for scaffold crosslinking, was obtained from Challenge Bioproducts Co. Fetal bovine serum (FBS) and phosphate-buffered saline (PBS) were obtained from Gibco. Plasmids encoding green fluorescent protein (pEGFP) and pVEGF were prepared at the Royan Institute, Iran. These plasmids were amplified in *E. coli* cultured in LB medium and purified using a Qiagen Giga kit (Hilden, Germany). The gene delivery vector, deoxycholic acid-modified branched PEI 1.8 kDa ($bPEI_{1.8}$-DA), was synthesized by our collaborators according to a previously established protocol [62]. HUVECs were obtained from the National Cell Bank of Iran (Pasteur Institute of Iran) and cultured in 75 cm^2 flasks using DMEM/F-12 supplemented with 10% heat-inactivated FBS. The culture environment was maintained at 37 °C within a humidified incubator containing 5% CO_2. All additional chemical and biological reagents were provided by the Pasteur Institute of Iran.

2.2. Preparation of $bPEI_{1.8}$-DA/pVEGF polyplexes and characterization

2.2.1. $bPEI_{1.8}$-DA polymer synthesis

$bPEI_{1.8}$-DA conjugate was synthesized by our collaborators according to a previously reported protocol [62] through conjugating the side-chain carboxyl group of DA to the terminal amine group of $bPEI_{1.8}$. Briefly, DA was first activated through a DCC/NHS coupling reaction. For this purpose, DA (2.0 g, 5.1 mmol) was dissolved in 50 ml of tetrahydrofuran (THF), and dicyclohexylcarbodiimide (DCC; 3.14 g, 15.2 mmol) and N-hydroxysuccinimide (NHS; 1.76 g, 15.3 mmol) were added to the solution to maintin a DA/DCC/NHS molar feed ratio of 1:3:3. After stirring at room temperature, the reaction mixture was filtered, concentrated by rotary evaporation, precipitated in cold hexane, and dried under vacuum oven at 30 °C. In the next step, the activated DA (0.2 g, 0.52 mmol) was reacted with $bPEI_{1.8}$ (0.3 g, 0.16 mmol) in methylene chloride at a 3:1 molar stoichiometric ratio of DA/$bPEI_{1.8}$. This reaction was stirred for 16 h at room temperature, and the solvent was then removed by rotary evaporation. The crude product was diluted in 0.1 M hydrochloric acid and purified by successive precipitation in a cold acetone-THF mixture (1:3 vol.%) and acetone-DEE mixture (1:3 vol.%). The dried product was then dissolved in deionized water, filtered, and lyophilized to obtain the dry conjugate. This vector was selected for the present study based on previous work demonstrating that DA-modified $bPEI_{1.8}$ conjugates can form stable nanocomplexes and improve nucleic acid delivery performance in HUVECs.

2.2.2. Plasmid extraction and purification

Plasmids encoding EGFP and VEGF were amplified in *E. coli* cultured in LB medium and purified according to the manufacturer's protocol. The plasmid concentration and purity were determined by measuring UV absorbance at 260 nm using a NanoDrop spectrophotometer. The purified plasmids were dissolved in Millipore water at a concentration of 5 μg μl^{-1} and stored at −20 °C.

2.2.3. Preparation of bPEI$_{1.8}$-DA-pDNA polyplexes

bPEI$_{1.8}$-DA/pVEGF polyplexes were prepared by mixing 50 µL of bPEI$_{1.8}$-DA solution containing 2 µg of polymer in PBS (pH 7.0) with 50 µl of pVEGF solution containing 1 µg of plasmid DNA in PBS (pH 7.0), corresponding to a polymer/plasmid weight ratio of 2. The mixture was gently pipetted and incubated for 1 h at room temperature to allow polyplex formation. For DLS characterization, 100 µl of the resulting polyplex suspension was diluted to 1 ml with double-distilled water, and the hydrodynamic diameter, reported as Z-average, was measured using a Cordouan Tech-VASCO$_2$ dynamic light scattering instrument.

2.2.4. Cell transfection study and polymer/plasmid DNA ratio optimization

To evaluate the gene delivery capability of the bPEI$_{1.8}$-DA vector and determine the appropriate polymer/-plasmid ratio for subsequent scaffold loading, transfection assays were first performed on HUVECs using pEGFP as a reporter plasmid. pEGFP/bPEI$_{1.8}$-DA polyplexes were prepared by gently adding 50 µl of pEGFP solution containing 1 µg of DNA in PBS (pH 7.0) to 50 µl of bPEI$_{1.8}$-DA polymer solution at different polymer/DNA weight ratios (0.5, 1, 1.5, 2, 2.5, 3, 4, 5, and 6). HUVECs were seeded in 24-well plates at a density of 5×10^4 cells/well and cultured for 24 h to reach approximately 70%–80% confluence before transfection. The culture medium was replaced with 400 µl of antibiotic-free low-serum medium containing 1% FBS. Then, 100 µl of pEGFP/bPEI$_{1.8}$-DA polyplex solution in PBS was added to each well. After 6 h of incubation at 37 °C, the medium was replaced with fresh complete medium containing 10% FBS. The plates were wrapped in aluminum foil and incubated for an additional 48 h at 37 °C. EGFP expression was then qualitatively observed using fluorescence microscopy (FM; Olympus IX71). The polymer/plasmid ratio that provided a suitable balance between EGFP expression and cytocompatibility was selected for the preparation of polyplexes used in the core of the fibers.

2.3. Fabrication of polyplex-loaded coaxial electrospun webs and threads

2.3.1. Preparation of core and shell solutions

To prepare the core solution for scaffold loading, 500 µl of bPEI$_{1.8}$-DA polymer solution containing 200 µg of polymer in PBS was slowly mixed with 500 µl of pVEGF solution containing 100 µg of plasmid DNA in PBS, corresponding to a polymer/plasmid weight ratio of 2. The mixture was gently pipetted, briefly vortexed, and incubated for 1 h at room temperature to allow polyplex formation. Based on our previous report [61], the shell solution was prepared at a total polymer concentration of 10% w/v by mixing gelatin/TFE and PCL/TFE solutions at a gelatin/PCL weight ratio of 70:30. The shell solution was stirred for approximately 12 h before electrospinning to ensure complete homogenization.

2.3.2. Coaxial electrospinning setup

The coaxial electrospinning setup used in this study was adapted from our previously established electrospinning platform, with modifications for the fabrication of aligned fibrous threads, as illustrated schematically in figure 1. The core and shell solutions were separately injected via the inner and outer capillaries of a coaxial nozzle (20 G and 14 G, respectively). Each capillary was directly connected to an individual syringe pump, eliminating the need for Teflon tubing. A high voltage was applied through a copper electrode attached directly to the coaxial nozzle.

To fabricate the core-shell nanofibers in a web format, a grounded rotating drum wrapped with aluminum foil was used as the collection surface (figure 1(a)). To obtain aligned core-shell fibrous bundles suitable for thread formation, the rotating drum was replaced with a grounded aluminum disk collector (12 cm diameter, 200 µm thickness), as shown in figure 1(b). The basic polymer composition and flow-rate range were selected based on our previous optimization of gelatin/PCL core–shell fibers [61]. Because the formation of core–shell fibers containing an aqueous core solution is highly sensitive to the balance between the core/shell flow rates and applied voltage, these parameters were adjusted to obtain a stable compound Taylor cone and continuous coaxial jet. After formation of a stable compound Taylor cone, a steady coaxial jet was ejected from the nozzle tip and accelerated toward the collector. During this process, solvent evaporation and jet stretching resulted in the deposition of core–shell composite nanofibers. Depending on the collector geometry, the deposited fibers formed either nonwoven fibrous webs or aligned fibrous bundles. The disk rotation speed was optimized to improve directional fiber deposition; among the tested conditions, 1300 rpm provided stable collection of aligned fibrous bundles at the peripheral edge of the disk.

For thread fabrication, aligned fiber bundles were collected from the disk edge after controlled accumulation. The collection time was adjusted to obtain fibrous threads within the target diameter range of 100–200 µm, which was required for future integration with the intended three-dimensional co-culture platform. A 15 min collection period was selected because it provided sufficient fiber accumulation, preserved bundle alignment, and produced cohesive threads within the desired diameter range. The collected fibrous bundle was then manually twisted between a fixed end and a rotating end to form a cohesive core–shell nanofibrous thread.

2.3.3. Crosslinking of the prepared scaffolds

After fabrication, the fibrous webs and threads were crosslinked with genipin. Genipin was selected

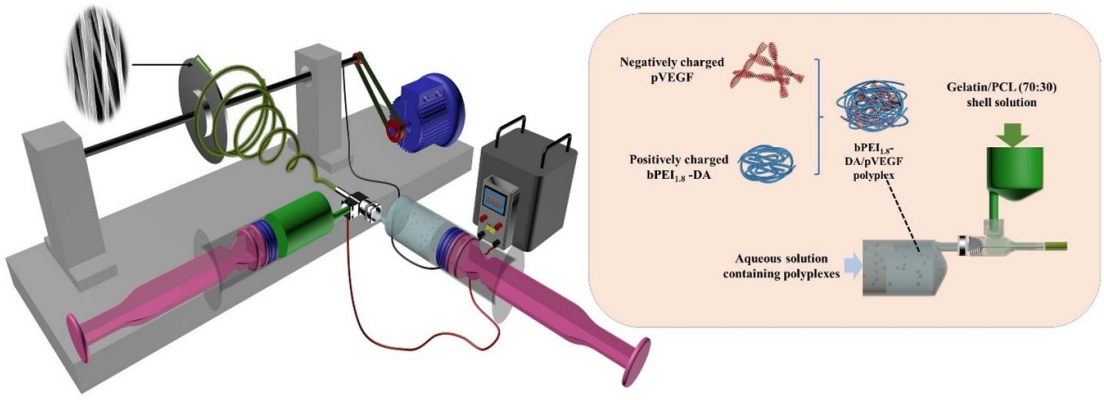

Figure 1. Schematic illustration of the modified coaxial electrospinning setup used to fabricate aligned core–shell fibrous bundles for thread formation. The aqueous core solution contained bPEI$_{1.8}$-DA/pVEGF polyplexes, while the shell solution consisted of gelatin/PCL (70:30). A rotating disk collector was used to obtain aligned fibers suitable for subsequent thread fabrication.

because of its relatively low molecular weight, which facilitates penetration into fibrous structures and promotes more uniform crosslinking [63]. The coaxial electrospun samples were entirely soaked in a 0.5% (w/v) genipin-ethanol solution and maintained at room temperature for three days. After crosslinking, the samples were washed three times with ethanol to remove unreacted genipin and then dried overnight at room temperature.

2.4. Morphological and mechanical characterization of the coaxial electrospun scaffolds

The morphology of the coaxial electrospun fibers and resulting threads were examined using scanning electron microscopy (SEM; AIS2100, Seron Technologies, Korea) at an accelerating voltage of 10 kV. Before imaging, the samples were sputter-coated with gold using an SCD 004 sputter coater (Balzers, Germany). Fiber diameter and diameter distribution were determined from SEM images using ImageJ software, based on 100–150 measurements for each sample group. To observe the encapsulation and distribution of polyplexes within the core-shell fibers, FM (Olympus IX71) was employed. For this analysis, RBITC-labeled bPEI$_{1.8}$-DA/pVEGF polyplexes were used in the core solution. The core-shell structure was further verified using transmission electron microscopy (TEM; EM10C, Zeiss) operating at an accelerating voltage of 100 kV.

Chemical changes associated with genipin crosslinking were analyzed using Fourier transform infrared spectroscopy (FTIR; NEXUS 670, Nicolet). FTIR spectra of crosslinked and non-crosslinked scaffolds were recorded over the wavenumber range of 4000–350 cm^{-1}. The mechanical performance of the electrospun threads was evaluated using a tensile testing instrument (Elima EMT-3050). Twenty-centimeter thread segments were weighed to determine their linear mass density in Tex, and tensile stress was expressed in cN/Tex. Tensile tests were conducted using a gauge length of 20 mm and a crosshead speed of 10 mm min^{-1}. Five independent thread specimens were tested for each group. Young's modulus was calculated from the slope of the initial linear elastic region of the stress–strain curve for each specimen. Ultimate tensile strength (UTS), elongation at break, and Young's modulus are reported as mean ± standard deviation (SD).

2.5. *In vitro* pVEGF release study from core-shell fibrous web and thread

The release of pVEGF polyplexes from the core–shell scaffolds was monitored using FITC-labeled bPEI$_{1.8}$-DA/pVEGF polyplexes. Briefly, bPEI$_{1.8}$-DA was conjugated through reaction of the FITC isothiocyanate groups with the primary amine groups of the polymer under dark conditions for 24 h at 4 °C. Unreacted FITC was removed by dialysis, followed by overnight lyophilization. FITC-labeled bPEI$_{1.8}$-DA was then complexed with pVEGF using the selected polymer/-plasmid ratio and incorporated into the scaffold core. Sterilized scaffold samples (3 cm web disks and 3 cm thread segments) were immersed in sealed microtubes containing 1.5 ml of PBS (pH 7.4). The tubes were wrapped in aluminum foil to minimize photobleaching and incubated at 37 °C. At predetermined time intervals (1, 3, and 6 h and 1, 2, 5, 8, 11, 16, 22, and 33 d), 100 µl of supernatant was withdrawn and replaced with an equal volume of fresh PBS. Fluorescence intensity was measured using a fluorescence plate reader at Ab/Em 484/525 nm. The released polyplex concentration was calculated using a standard calibration curve prepared from FITC-conjugated bPEI$_{1.8}$-DA/pVEGF polyplexes. At the end of the release study, residual polyplexes retained within the scaffolds were extracted using a dichloromethane/acetic acid solvent system followed

by phase separation with PBS. After vortexing (3 min) and centrifugation (4000 rpm, 5 min), 100 µl of the PBS supernatant was withdrawn and analyzed fluorometrically to calculate the cumulative loading efficiency. All release assays were performed in triplicate, and the results are expressed as mean ± SD.

2.6. *In vitro* cytocompatibility evaluation

The cytocompatibility of the core–shell fibrous webs was evaluated using HUVECs cultured in DMEM/F-12 supplemented with 10% FBS under standard conditions (37 °C and 5% CO_2). Circular scaffold samples (14 mm diameter) were sterilized under UV irradiation for 2 h, washed with PBS, and pre-incubated in culture medium for 24 h. HUVECs were then seeded onto the scaffolds in 24-well plates at a density of 5×10^4 cells/well, and the culture medium was replaced every 2 d. Cell attachment and morphology were examined by SEM after 1 d of culture. The cell-seeded scaffolds were gently rinsed with PBS, fixed with 3% glutaraldehyde for 1 h, dehydrated through a graded ethanol series (30–100%; 10 min at each concentration), and air-dried before imaging. Cell viability and proliferation were assessed using the MTT assay after 1, 4, and 7 d of culture. At each time point, 200 µl of MTT solution ($0.5\ g\ l^{-1}$) was added to each well and incubated for 4 h at 37 °C. The MTT medium was then removed, and the resulting formazan crystals were dissolved in DMSO. Absorbance was measured at 570 nm using a microplate reader. HUVECs cultured in tissue culture plate wells without scaffolds were used as the control group. All experiments were performed in quadruplicate.

2.7. Evaluation of gene expression activity and VEGF secretion

To evaluate whether scaffold incorporation and subsequent release affected the gene expression capability of the polyplexes, a qualitative reporter-gene assay was performed using pEGFP. Based on the optimized polymer/plasmid ratio determined in section 2.2.4, pEGFP/$bPEI_{1.8}$-DA polyplexes were prepared and incorporated into the core of the core–shell fibrous scaffolds under the same fabrication conditions used for pVEGF polyplex loading. The pEGFP polyplex-loaded scaffolds were incubated in culture medium, and the release medium containing the released pEGFP/$bPEI_{1.8}$-DA polyplexes was collected after 2 d and used for HUVEC transfection. The transfection procedure was performed under the same conditions described in section 2.2.4. After 48 h of post-transfection incubation, EGFP expression was qualitatively observed using FM. This assay was used to assess the retained gene expression capability of the released polyplexes after scaffold incorporation and release.

To further evaluate the biological activity of the pVEGF polyplex-loaded scaffolds, VEGF protein secretion was quantified in HUVEC-conditioned culture medium using a Human VEGF sandwich ELISA kit (abs510008-96T) according to the manufacturer's instructions. HUVECs were seeded in 24-well plates at 5×10^4 cells/well and cultured in 500 µl of medium. The experimental groups included untreated HUVECs as the control, crosslinked BSA-loaded webs, free $bPEI_{1.8}$-DA-pVEGF polyplexes, crosslinked pVEGF polyplex-loaded webs, and crosslinked pVEGF polyplex-loaded threads. Conditioned media were collected at days 1, 3, 7, 14, 21, and 28 and stored at −80 °C until analysis. For each sample, 100 µl of conditioned medium was used, and absorbance was measured at 450 nm with wavelength correction at 540/570 nm. VEGF concentrations were calculated from the standard curve and reported as pg/ml. Experiments were performed in triplicate.

2.8. Statistical analysis

All quantitative data are presented as mean ± SD. Statistical analyses were performed using GraphPad Prism software. Comparisons between two independent groups, including the mechanical properties of non-crosslinked and genipin-crosslinked threads, were performed using an unpaired two-tailed Student's *t*-test. For comparisons among three or more groups involving a single independent factor, ordinary one-way analysis of variance (ANOVA) followed by Tukey's multiple-comparisons test was used. Data involving both experimental group and time, including the MTT and VEGF ELISA results, were analyzed using ordinary two-way ANOVA followed by Tukey's multiple-comparisons test. Where release values were statistically compared between two scaffold groups at a specific time point, an unpaired two-tailed Student's *t*-test was applied. Differences were considered statistically significant at $p < 0.05$.

3. Results

3.1. Fabrication and characterization of core-shell fibrous thread

Coaxial electrospinning utilizing a rotating disk collector enabled the successful fabrication of core-shell fibers loaded with $bPEI_{1.8}$-DA/pVEGF polyplexes in the core and gelatin/PCL hybrid (70:30) as the shell layer. Bead-free fibers were obtained through the formation of a stable compound Taylor cone under the optimized spinning parameters. For the fabrication of random fibrous webs, the electrospinning parameters were selected based on our previously established gelatin/PCL core–shell scaffold platform: inner flow rate of 0.2 ml h^{-1}, outer flow rate of 0.7 ml h^{-1}, applied voltage of 14 kV, and collection distance of 12 cm [61]. For aligned fiber collection and thread fabrication, a stable compound Taylor cone and continuous coaxial jet were obtained using an inner flow

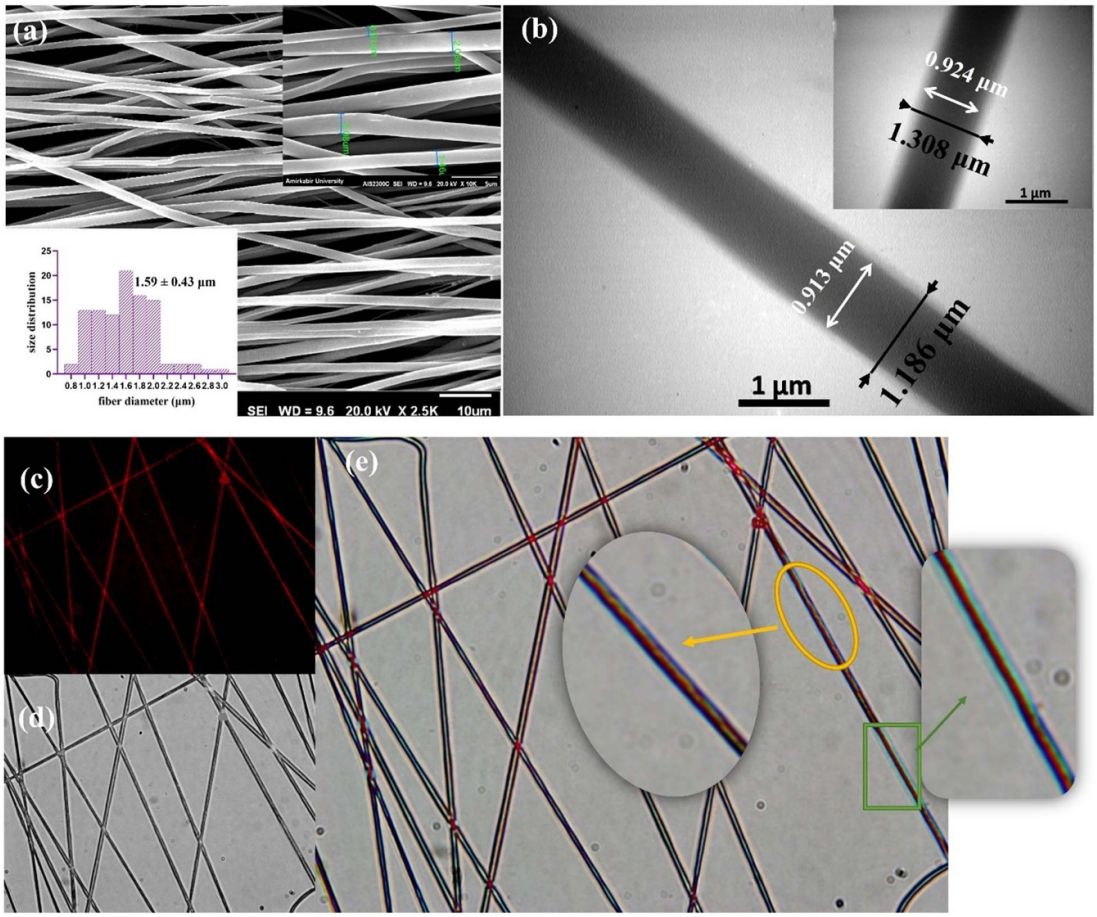

Figure 2. Morphological characterization of aligned core–shell fibers containing bPEI$_{1.8}$-DA/pVEGF polyplexes. (a) Representative SEM images and fiber-diameter distribution of the aligned core–shell fibers (b) TEM images showing the core–shell morphology, with the core and overall fiber diameters indicated by arrows. (c) FM image of the core-shell fibers in which RBITC was used to stain polyplexes. FM image showing the homogeneous distribution of RBITC-conjugated-bPEI$_{1.8}$-DA/pVEGF within the fiber core. (d) Corresponding bright-field image of the same fibers. (e) Merged fluorescence and bright-field image showing the spatial association of the RBITC-labeled polyplexes with the core–shell fibers.

rate of 0.1 ml h^{-1} and an applied voltage of 10 kV, while maintaining the outer flow rate at 0.7 ml h^{-1} and the collection distance at 12 cm. SEM images of the coaxially spun fibers taken from the rotating disk collector showed smooth, continuous, and bead-free morphologies (figure 2(a)). Among the tested disk rotation speeds, 1300 rpm produced aligned fibrous bundles suitable for subsequent thread formation. Under these conditions, the mean fiber diameter was 1.59 ± 0.43 µm.

TEM images showed a continuous coaxial morphology with distinguishable core and shell regions (figure 2(b)), confirming formation of the core–shell fiber structure. FM was used to evaluate the incorporation and distribution of RBITC-labeled bPEI$_{1.8}$-DA/pVEGF polyplexes within the fibers. A red fluorescence signal was observed along the fiber length (figure 2(c)), indicating incorporation and distribution of the labeled polyplexes within the fibrous structures. The corresponding bright-field image is shown in figure 2(d), and the merged image in figure 2(e) demonstrates the spatial association of the fluorescence signal with the fibers.

The aligned fibrous bundles were subsequently twisted into cohesive core–shell nanofibrous threads. The final thread diameter was controlled by the fiber collection time. Increasing the collection time from 5 to 10, 15, and 20 min increased the thread diameter from 77 µm to 108, 148, and 261 µm, respectively. A collection time of 15 min was selected for subsequent experiments because it produced continuous and handleable threads with a diameter of approximately 148 µm, within the predefined target range of 100–200 µm. SEM images were used to examine fiber orientation and surface morphology within the integrated threads (figure 3). The fibers largely preserved their aligned arrangement after collection and twisting, and exhibited smooth, bead-free surfaces. SEM observations after genipin crosslinking (figures 3(d) and (e)) showed the overall thread morphology and fibrous alignment were preserved. A slight increase in fiber diameter was observed after crosslinking.

FTIR spectroscopy was used to compare the chemical characteristics of non-crosslinked and genipin-crosslinked fibrous threads (figure 4(a)). Both spectra exhibited the characteristic absorption

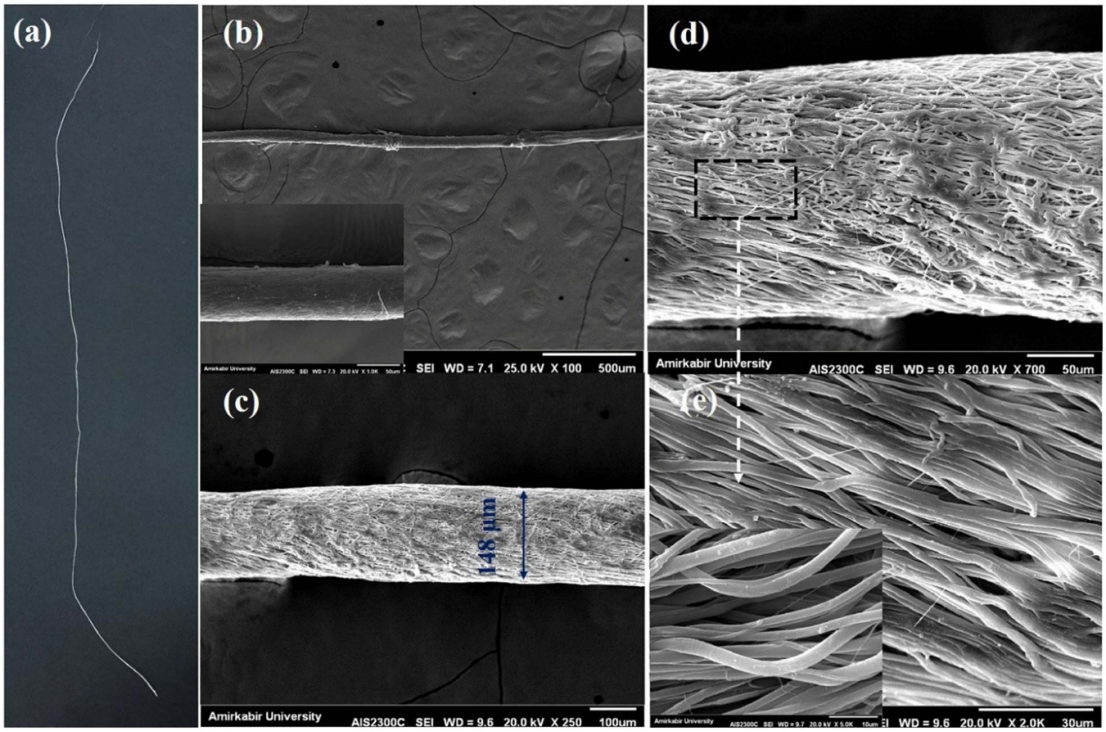

Figure 3. Morphological characterization of the fabricated core–shell fibrous thread. (a) Digital photograph of a representative fibrous thread. (b), (c) SEM images of the core–shell fibrous thread at different magnifications, showing the overall thread morphology and a thread diameter of approximately 148 µm. (d), (e) SEM images of the genipin-crosslinked fibrous thread at different magnifications, showing preservation of the aligned fibrous structure after crosslinking. The inset in panel (e) presents a higher-magnification view of the individual fibers.

bands of PCL, including the ester carbonyl stretching band at approximately 1730 cm^{-1}, asymmetric and symmetric CH_2 stretching bands at 2949 and 2865 cm^{-1}, respectively, and bands at approximately 1293, 1240, and 1170 cm^{-1} associated with C–O, C–C, and C–O–C stretching vibrations. The characteristic gelatin-related bands were observed at approximately 1640 cm^{-1} for Amide I, primarily associated with C=O stretching, and 1540 cm^{-1} for Amide II, associated mainly with N–H bending and C–N stretching [64, 65]. These bands serve as sensitive indicators of the polypeptide secondary structure within the gelatin-based threads [66]. Additional bands were detected near 3330 cm^{-1} for Amide A and around 1240 cm^{-1} for Amide III, although the latter overlapped with the C–O–C absorption band of PCL. Following genipin crosslinking, changes in the intensity and spectral profile of the gelatin-associated amide bands were observed, particularly in the Amide A, Amide I, and Amide II regions [67]. These spectral changes were consistent with chemical modification of the gelatin-containing fibrous threads after genipin treatment [67, 68].

The tensile behavior of the fabricated core–shell fibrous threads was evaluated using stress–strain measurements, and representative curves are shown in figure 4(b). Young's modulus was determined from the slope of the initial linear elastic region of the stress–strain curve for each specimen. Both non-crosslinked and genipin-crosslinked pVEGF polyplex-loaded threads exhibited a characteristic bilinear deformation profile, consisting of an initial linear elastic region followed by a nonlinear deformation region. The non-crosslinked threads exhibited a Young's modulus of 37.13 cN/Tex, an UTS of 1.80 cN/Tex, and an elongation at break of 13.89%. Following genipin crosslinking, Young's modulus increased to 49.81 cN/Tex. The elongation at break decreased significantly from 13.89% to 8.18% after crosslinking ($p < 0.05$), whereas the UTS increased slightly from 1.80 to 1.94 cN/Tex, with no statistically significant difference between the groups ($p > 0.05$).

3.2. Cell transfection study

The transfection capability of the $bPEI_{1.8}$-DA vector was evaluated using pEGFP as a reporter plasmid to determine the appropriate polymer/plasmid DNA ratio for subsequent scaffold loading. The aim of this preliminary optimization was to identify a formulation that provided an appropriate balance between EGFP expression and cytocompatibility. HUVECs were incubated with $bPEI_{1.8}$-DA/pEGFP polyplexes prepared at different polymer/plasmid ratios for 6 h, and EGFP expression and cell morphology were qualitatively examined by FM. Initial screening was performed using polymer/DNA ratios of 1, 2, 3, 4, 5, and 6. FM observations showed that higher polymer/DNA ratios, particularly 4, 5, and 6, were associated with

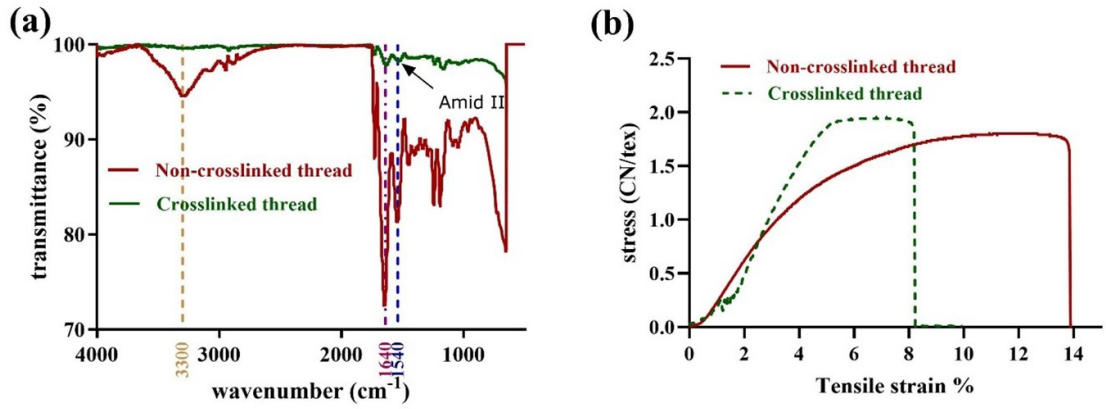

Figure 4. Chemical and mechanical characterization of the core–shell fibrous threads. (a) FTIR spectra of non-crosslinked and crosslinked fibrous threads, showing changes in the gelatin-associated amide bands after crosslinking. (b) Representative tensile stress–strain curves of non-crosslinked and crosslinked fibrous threads. Young's modulus was calculated from the slope of the initial linear elastic region of each stress–strain curve.

increased cytotoxicity, as indicated by reduced cell density and altered cell morphology. Therefore, the transfection assay was repeated using lower ratios of 1, 1.5, 2, 2.5, and 3 to further refine the formulation. Among these conditions, lower apparent cytotoxicity was observed at ratios between 1 and 2. To identify the most suitable condition, additional assays were performed at ratios of 1, 1.5, and 2 using two different bPEI$_{1.8}$-DA amounts, 0.5 and 1 μg per well. All transfection experiments were performed in triplicate. Among the tested conditions, polyplexes prepared at a polymer/DNA weight ratio of 2 using 0.5 μg of bPEI$_{1.8}$-DA per well showed the most favorable qualitative balance between EGFP expression and cell morphology. As shown in figure 5, HUVECs treated with bPEI$_{1.8}$-DA/ pEGFP polyplexes prepared under this condition showed detectable EGFP expression, confirming successful reporter gene delivery. Based on these results, the polymer/DNA ratio of 2 with 0.5 μg of bPEI$_{1.8}$-DA per well was selected for the preparation of pVEGF polyplexes used in the core of the coaxial electrospun fibers. The DLS results showed that bPEI$_{1.8}$-DA condensed the plasmids into nanoscale polyplexes with diameters in the range of 65–100 nm, confirming successful polyplex formation suitable for incorporation into the core of the fibrous scaffolds.

3.3. Release study of bPEI$_{1.8}$-DA/pDNA polyplexes

A fluorescence plate reader was used to monitor the release of FITC-conjugated bPEI$_{1.8}$-DA-pVEGF polyplexes over 33 d. The release behavior was evaluated from core–shell nanofibrous scaffolds fabricated in both web and thread configurations. All measurements were performed in triplicate, and data are presented as mean ± SD. A standard calibration curve was first generated using different concentrations of FITC-conjugated bPEI$_{1.8}$-DA/pVEGF polyplexes. Fluorescence intensity was measured at an excitation wavelength of 484 nm and an emission wavelength of 525 nm, as shown in figure 6(a). The cumulative release profiles and representative release values are presented in figures 6(b)–(d) and table 1. For clearer interpretation, the 33 d release period was divided into three stages: Stage I, corresponding to the initial burst release within the first 3 h; Stage II, representing the sustained release phase up to day 11; and Stage III, corresponding to the final slow-release phase up to day 33.

Figure 6(b) illustrates the cumulative release profiles from non-crosslinked pVEGF polyplex-loaded webs, crosslinked pVEGF polyplex-loaded webs, and crosslinked BSA-loaded webs as a reference biomolecule-loaded scaffold. According to table 1, the initial burst release of FITC-polyplexes from non-crosslinked webs reached 44.85 ± 8.87% within the first 3 h, whereas crosslinked webs released a significantly lower amount of 25.50 ± 7.81% during the same period ($p < 0.05$). After this initial stage, cumulative release reached 71.19 ± 11.30% and 46.20 ± 8.97% from non-crosslinked and crosslinked webs, respectively. At the end of the 33 d period, the cumulative release values were 82.99 ± 15.45% and 57.38 ± 9.39% for non-crosslinked and crosslinked webs, respectively. The final stage showed minimal further release, concluding at 82.99 ± 15.45% and 57.38 ± 9.39%, respectively. The release of BSA from crosslinked webs was also evaluated as a reference biomolecule-loaded system. BSA release from crosslinked webs reached 54.96 ± 6.44% at 3 h, 86.45 ± 0.38% by day 11, and 93.34 ± 0.07% after 33 d. At all three representative time points, the cumulative release of polyplexes from crosslinked webs was lower than the corresponding BSA release.

The release profiles from the thread configuration were further analyzed, as shown in figure 6(c). The crosslinked BSA-loaded thread was included as an additional reference biomolecule-loaded thread. BSA release from crosslinked threads reached 33.00 ± 2.23% at 3 h, 60.10 ± 1.07% by day 11, and

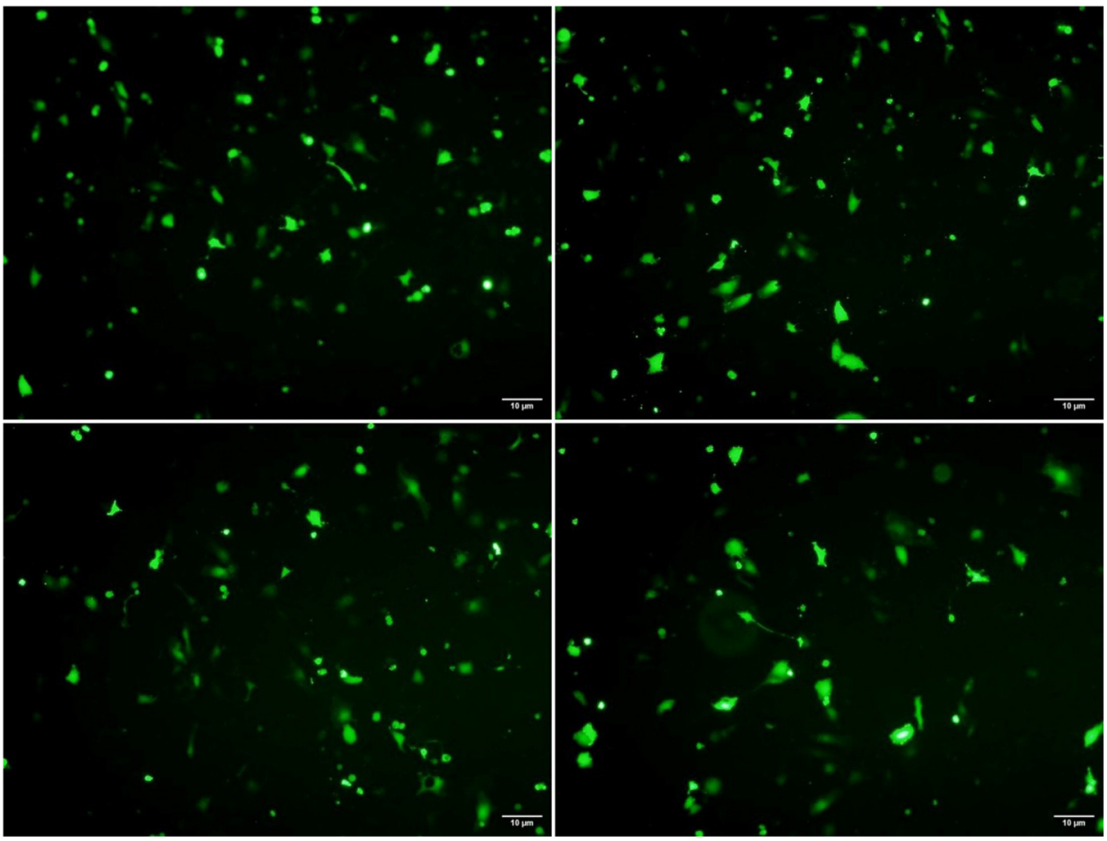

Figure 5. Representative fluorescence microscopy images showing EGFP expression in HUVECs after transfection with bPEI$_{1.8}$-DA/pEGFP polyplexes prepared at a polymer/DNA weight ratio of 2. The presence of EGFP-positive cells qualitatively demonstrates reporter gene expression under the selected polyplex formulation condition.

71.07 ± 2.26% after 33 d. The cumulative release of FITC-polyplexes from crosslinked threads was 16.59 ± 6.54% at 3 h, 30.32 ± 11.37% at day 11, and 41.64 ± 13.57% at day 33. These values were lower than those observed for crosslinked pVEGF polyplex-loaded webs at the same time points. The cumulative amount of released pVEGF polyplexes was also expressed in ng over the 33 d period (figure 6(d)). Throughout the study, the cumulative released amount from crosslinked pVEGF polyplex-loaded threads remained lower than that from the corresponding crosslinked webs.

3.4. *In vitro* cytocompatibility

The cytocompatibility of the coaxial electrospun scaffolds was evaluated by examining HUVEC attachment, morphology, and proliferation. SEM images (figures 7(a) and (b)) showed that HUVECs adhered to both non-crosslinked and genipin-crosslinked core–shell fibrous webs after 1 d of culture. On the non-crosslinked scaffolds, the cells exhibited elongated and polygonal morphologies with cytoplasmic extensions interacting with the surrounding nanofibers. HUVECs cultured on the crosslinked scaffolds also remained attached and displayed more extensive spreading, with flattened cell bodies and sheet-like regions bridging adjacent fibers. The MTT assay results showed a time-dependent increase in HUVEC metabolic activity in all groups from day 1 to day 7 (figure 7(c)). At day 7, all scaffold groups exhibited significantly higher absorbance values than the control ($^{****}p < 0.0001$). The crosslinked pVEGF polyplex-loaded scaffolds exhibited higher metabolic activity than the corresponding non-crosslinked pVEGF polyplex-loaded scaffolds at days 4 and 7, with statistically significant differences at both time points ($^{**}p < 0.01$ at day 4 and $^{****}p < 0.0001$ at day 7). At day 7, the crosslinked pVEGF polyplex-loaded scaffold also showed significantly higher metabolic activity than the crosslinked BSA-loaded scaffold ($^{****}p < 0.0001$).

3.5. Gene expression capability and VEGF secretion from HUVECs

To evaluate whether scaffold incorporation and subsequent release affected the functional activity of the polyplexes, a qualitative reporter-gene assay was performed using pEGFP. As shown in figures 8(a) and (b), EGFP-positive HUVECs were observed after incubation with pEGFP/bPEI$_{1.8}$-DA polyplexes released from the core–shell fibrous scaffolds. These observations showed that the released polyplexes retained the ability to mediate reporter-gene expression after scaffold fabrication and release.

Table 1. Cumulative release percentages of BSA and FITC-conjugated $bPEI_{1.8}$-DA/pVEGF polyplexes from core–shell fibrous webs and threads at three representative release stages. Values are presented as mean ± SD. FITC-conjugated $bPEI_{1.8}$-DA/pVEGF polyplexes are abbreviated as FITC-polyplexes in the table. '–' indicates conditions that were not evaluated.

		Cumulative release (%)					
		Stage I (3 h)		Stage II (11 d)		Stage III (33 d)	
Released biomolecule	Type of scaffold	Non-crosslinked	Crosslinked	Non-crosslinked	Crosslinked	Non-crosslinked	Crosslinked
BSA	Web	62.73 ± 2.60	54.96 ± 6.44	86.84 ± 0.72	86.45 ± 0.38	93.70 ± 0.53	93.34 ± 0.07
FITC-polyplexes	Web	44.85 ± 8.87	25.50 ± 7.81	71.19 ± 11.30	46.20 ± 8.97	82.99 ± 15.45	57.38 ± 9.39
BSA	Thread	—	33 ± 2.23	—	60.10 ± 1.07	—	71.07 ± 2.26
FITC-polyplexes	Thread	—	16.59 ± 6.54	—	30.32 ± 11.37	—	41.64 ± 13.57

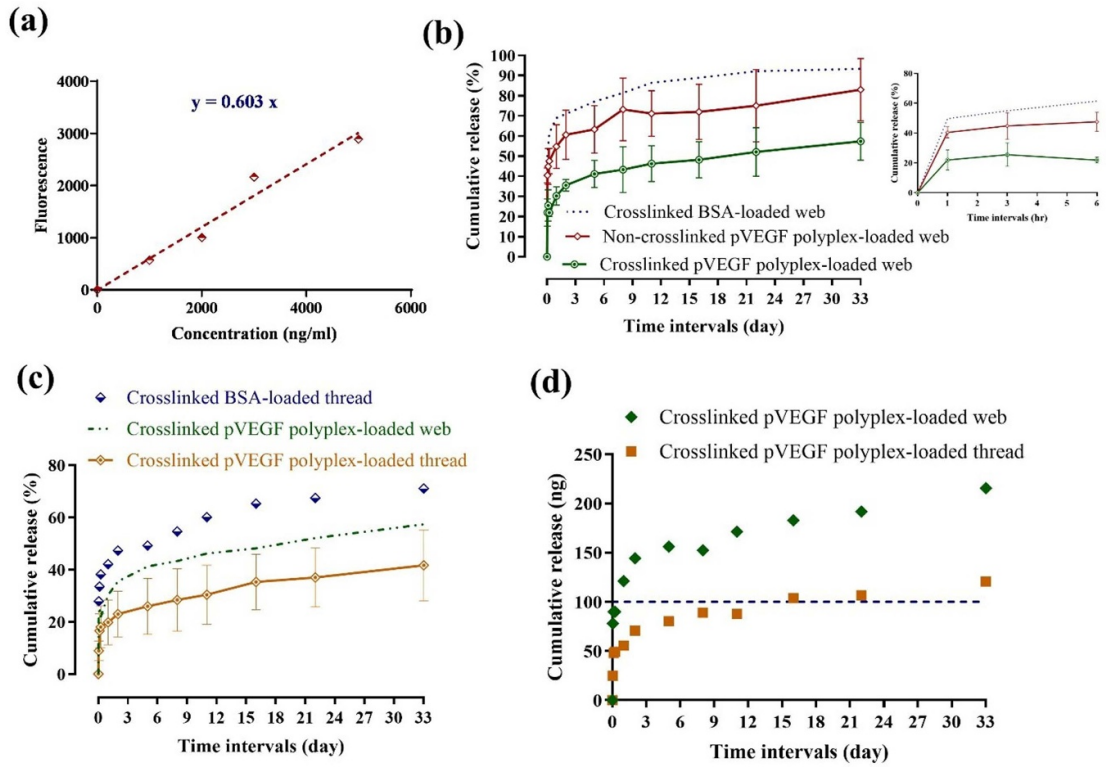

Figure 6. Release profiles of BSA and pVEGF polyplexes from core–shell fibrous webs and threads. (a) Standard calibration curve of fluorescence intensity versus concentration of FITC-conjugated $bPEI_{1.8}$-DA/pVEGF polyplexes (b) Cumulative release profiles from crosslinked BSA-loaded webs, non-crosslinked pVEGF polyplex-loaded webs, and crosslinked pVEGF polyplex-loaded webs. The inset shows the initial release behavior during the first 6 h. (c) Cumulative release profiles from crosslinked BSA-loaded threads, crosslinked pVEGF polyplex-loaded webs, and crosslinked pVEGF polyplex-loaded threads. (d) Cumulative amount of released pVEGF polyplexes, expressed in ng, from crosslinked webs and threads. The dashed line represents the threshold-guided reference level of 100 ng. Data are presented as mean ± SD.

VEGF secretion by HUVECs was subsequently quantified by ELISA in conditioned culture medium over 28 d (figure 8(c)). The control and crosslinked BSA-loaded web groups maintained relatively low VEGF concentrations throughout the culture period. In contrast, higher VEGF concentrations were measured in all groups containing $bPEI_{1.8}$-DA/pVEGF polyplexes. The free $bPEI_{1.8}$-DA/pVEGF polyplex group showed an early increase in VEGF secretion, reaching a maximum concentration of 906.75 ± 91.87 pg ml^{-1} at day 3, followed by a progressive decrease to 112.38 ± 26.98 pg ml^{-1} at day 28. For the crosslinked pVEGF polyplex-loaded web, VEGF concentration increased from 264.32 ± 31.38 pg ml^{-1} at day 1 to a maximum of 1093.26 ± 104.69 pg ml^{-1} at day 7 and subsequently decreased to 360.15 ± 55.38 pg ml^{-1} at day 28. The crosslinked pVEGF polyplex-loaded thread showed a later maximum VEGF concentration. VEGF secretion increased from 140.36 ± 21.81 pg ml^{-1} at day 1–696.85 ± 77.89 pg ml^{-1} at day 7 and reached its highest value of 1045.95 ± 112.50 pg ml^{-1} at day 14. Concentrations of 888.50 ± 91.07 and 604.06 ± 75.39 pg ml^{-1} were measured at days 21 and 28, respectively.

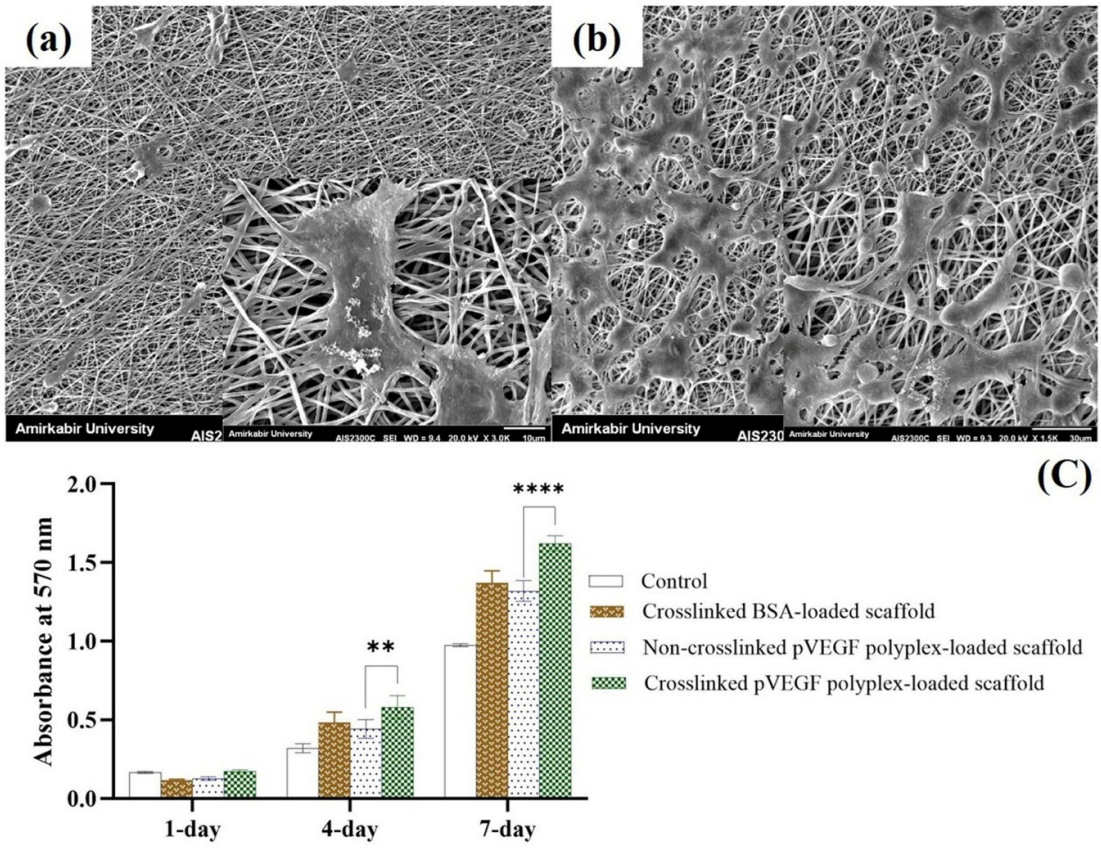

Figure 7. *In vitro* cytocompatibility of core–shell fibrous scaffolds. SEM images of HUVEC adhesion and spreading on (a) non-crosslinked and (b) genipin-crosslinked scaffolds after 1 d of culture. (c) MTT assay of HUVECs cultured on tissue culture plate wells as the control, crosslinked BSA-loaded scaffolds, non-crosslinked pVEGF polyplex-loaded scaffolds, and crosslinked pVEGF polyplex-loaded scaffolds after 1, 4, and 7 d of culture. Data are presented as mean ± SD (n = 4). Statistical analysis was performed using ordinary two-way ANOVA followed by Tukey's multiple comparisons test. Statistical brackets indicate comparisons between non-crosslinked and crosslinked pVEGF polyplex-loaded scaffolds at the same time point. $^{**}p < 0.01$ and $^{****}p < 0.0001$.

Ordinary two-way ANOVA followed by Tukey's multiple-comparisons test showed significant effects of experimental group, culture time, and their interaction on VEGF secretion ($p < 0.0001$). The crosslinked pVEGF polyplex-loaded web exhibited a significantly higher VEGF concentration than the corresponding thread group at day 7 ($^{****}p < 0.0001$). In contrast, VEGF concentrations in the thread group were significantly higher than those in the web group at days 21 and 28 ($^{****}p < 0.0001$).

4. Discussion

Combining polymeric scaffolds with angiogenic gene-vector complexes provides a promising approach that can maintain their desired levels to control the rate and extent of angiogenesis according to the needs of the specific tissue being engineered. The effectiveness of this strategy depends on coordinated optimization of the type and concentration of angiogenic agents and the architecture of the delivery scaffold. Although VEGF is a key regulator of angiogenesis, excessive or poorly controlled VEGF exposure may result in immature, malformed, or hemangioma-like vascular structures. Therefore, scaffold-mediated VEGF gene delivery offers a potential means of maintaining localized and sustained VEGF production while reducing uncontrolled exposure. In the present study, aligned core–shell fibrous threads were developed to encapsulate $bPEI_{1.8}$-DA/pVEGF polyplexes and regulate their release over an extended period. The thread configuration was selected to combine directional fibrous architecture with localized gene-vector delivery. In future applications, these threads may be integrated into three-dimensional co-culture systems as guidance structures for microvessel-like organization while providing sustained delivery of angiogenic gene vectors.

To transfect pVEGF into cells, we used DA-modified $bPEI_{1.8}$ as one of the newest gene delivery vectors. Cationic polymeric vectors offer several advantages over viral systems, including easier preparation, lower immunogenicity, and greater structural tunability; however, their clinical translation is still limited by the need to balance transfection efficiency and cytotoxicity [69, 70]. High-molecular-weight PEI, such as $bPEI_{25}$, generally provides efficient

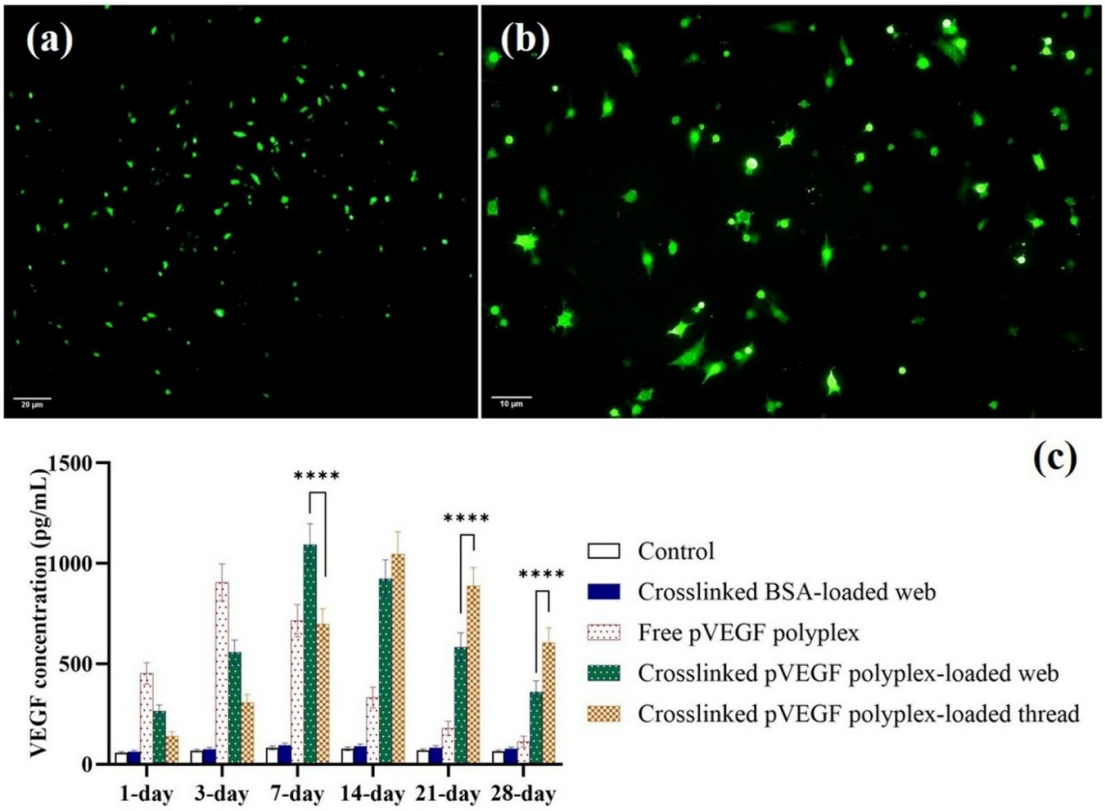

Figure 8. Evaluation of gene expression capability and VEGF secretion after scaffold-mediated polyplex delivery. (a) and (b) Representative FM images showing EGFP expression in HUVECs after incubation with pEGFP/bPEI$_{1.8}$-DA polyplexes released from core–shell fibrous scaffolds. (c) VEGF protein secretion from HUVECs cultured with different formulations, quantified by ELISA in conditioned culture medium over 28 d.

gene delivery but is associated with considerable cytotoxicity, whereas low-molecular-weight bPEI$_{1.8}$ exhibits a more favorable cytocompatibility profile but lower transfection efficiency. To address this limitation, our collaborators previously developed deoxycholic acid-modified bPEI$_{1.8}$ conjugates and demonstrated improved nucleic acid delivery performance in HUVECs [62]. The improved performance of bPEI$_{1.8}$-DA was attributed to its ability to form stable nanocomplexes, enhance cellular uptake, and facilitate intracellular cargo release while maintaining a more favorable cytotoxicity profile than bPEI$_{25}$. Based on these previous findings, bPEI$_{1.8}$-DA was selected in the present study as a suitable carrier for pVEGF delivery.

Because the current study involved incorporation of pDNA polyplexes into the core of electrospun fibrous scaffolds, the polymer/plasmid DNA weight ratio was first optimized using pEGFP as a reporter plasmid. This preliminary optimization was performed to identify a formulation that could provide effective reporter gene expression while minimizing cytotoxicity in HUVECs. The results showed that higher polymer/DNA ratios were associated with greater cytotoxicity, whereas a ratio of 2 using 0.5 μg of bPEI$_{1.8}$-DA per well provided the most favorable qualitative balance between EGFP expression and cell morphology. This formulation was therefore selected for preparation of bPEI$_{1.8}$-DA/pVEGF polyplexes and their subsequent incorporation into the core of the coaxial electrospun fibers. The present work extends the previously established gene delivery capability of bPEI$_{1.8}$-DA to a core–shell fibrous thread platform designed for sustained pVEGF polyplex delivery. The retained EGFP expression after scaffold release and the prolonged VEGF secretion observed in HUVECs indicate that this platform preserved the functional activity of the incorporated polyplexes while extending their availability over time.

In this study, coaxial electrospinning was employed to encapsulate bPEI$_{1.8}$-DA/pVEGF polyplexes within the aqueous fiber core and to protect the gene-vector complexes during scaffold fabrication. The use of an aqueous core makes coaxial electrospinning particularly sensitive to the balance among the core and shell flow rates, applied voltage, and collector configuration; therefore, these parameters must be adjusted carefully to maintain a stable compound Taylor cone and continuous coaxial jet. The initial shell composition and processing window were selected based on our previous study, in which crosslinked gelatin/PCL core–shell fibers with a 70:30 shell composition exhibited favorable mechanical properties, cellular responses, and biphasic release

of BSA and EGF as model biomolecules [61]. Based on these findings, gelatin/PCL (70:30) was selected as the shell composition in the present study.

The electrospinning setup was subsequently modified to convert the conventional non-woven web configuration into aligned fibrous threads with a target diameter of 100–200 μm. A grounded rotating aluminum disk was used instead of the conventional drum collector to promote directional fiber deposition at the disk periphery. For thread fabrication, the inner flow rate and applied voltage were reduced relative to the web-processing conditions to preserve the stability of the compound Taylor cone during disk collection. In addition, the disk rotation speed was optimized, with 1300 rpm providing aligned fibrous bundles suitable for thread formation. The collection time was then controlled to regulate thread thickness; a 15 min collection period produced continuous and handleable threads with a diameter of approximately 148 μm, within the predefined range intended for future integration with a three-dimensional co-culture platform.

In the present study, an aqueous solution of $bPEI_{1.8}$-DA/pVEGF polyplexes was successfully incorporated into the core of gelatin/PCL (70:30) fibers using a modified coaxial electrospinning equipped with a rotating disk collector. SEM observations showed that the resulting threads consisted of smooth, bead-free, and highly aligned fibers. The directional alignment was promoted by fiber deposition along the peripheral edge of the rotating disk, where the localized electric field and collector motion favored the formation of aligned fibrous bundles. FM showed a continuous red signal along the fiber length, indicating successful incorporation and relatively uniform distribution of the RBITC-labeled polyplexes within the fibrous structures. The corresponding merged fluorescence and bright-field images further demonstrated the spatial association of the labeled polyplexes with the fibers. In parallel, TEM revealed distinguishable inner and outer regions within individual fibers, providing direct morphological evidence of the core–shell architecture. Taken together, the SEM, FM, and TEM observations support the successful formation of aligned core–shell fibers containing polyplexes within the internal compartment.

Because gelatin is hydrophilic and susceptible to swelling and partial dissolution in aqueous environments, crosslinking was performed to improve the structural stability of the fibrous threads. Residual conventional crosslinking agents may cause considerable cytotoxicity if they are not completely removed from the final scaffold. Genipin was therefore selected as a comparatively biocompatible crosslinker because of its substantially lower cytotoxicity [71, 72]. Its reaction with the primary amino groups of gelatin promotes the formation of intermolecular crosslinks, thereby reducing gelatin solubility and stabilizing the fibrous network. SEM observations showed that the genipin-treated threads retained their overall fibrous morphology and aligned organization after crosslinking. The slight increase in fiber diameter observed after treatment was likely associated with swelling of the gelatin-containing fibers during exposure to the aqueous crosslinking environment. In addition, the changes detected in the gelatin-associated Amide A, Amide I, and Amide II regions of the FTIR spectra were consistent with chemical modification of gelatin and supported the formation of a genipin-crosslinked network.

The mechanical behavior of the core–shell fibrous threads is an important consideration for their handling and potential integration into tissue-engineering systems. This behavior is governed by the combined contribution of the gelatin/PCL shell composition, fiber alignment, thread architecture, and crosslinking state. In our previous study, increasing the gelatin fraction in gelatin/PCL core–shell fibers was associated with a higher Young's modulus, and the crosslinked gelatin/PCL (70:30) formulation showed a favorable balance of stiffness and tensile performance [61]. It was assumed that combining gelatin and PCL fibers could enhance tensile properties. Gelatin fibers are characterized by high stiffness, high modulus, and limited extensibility, PCL fibers provide necessary flexibility and softness. This assumption is based on the premise that increased crystallinity often leads to improved mechanical strength in polymeric materials, and gelatin's contribution to crystallinity would leverage this relationship [73, 74]. Fiber orientation is also expected to contribute to the mechanical response because load transfer occurs more efficiently when fibers are oriented along the tensile direction [75]. In the present study, both non-crosslinked and genipin-crosslinked threads exhibited a bilinear tensile response, reflecting the combined deformation of individual fibers and their interactions within the twisted bundle. Genipin crosslinking increased Young's modulus from 37.13 to 49.81 cN/Tex, indicating a stiffer thread structure, while elongation at break decreased significantly. In contrast, the change in UTS was small and not statistically significant. These findings suggest that crosslinking primarily altered the elastic response and deformability of the threads rather than their maximum load-bearing capacity. The increase in stiffness and reduction in extensibility may be related to the formation of covalent crosslinks within the gelatin phase and improved stabilization of fiber–fiber contact points, which restricted molecular and inter-fiber mobility.

Cell adhesion and proliferation are important indicators of scaffold cytocompatibility and of the ability of a biomaterial to support cell-scaffold interactions. SEM observations showed that HUVECs adhered to both non-crosslinked and genipin-crosslinked fibrous webs, while the crosslinked

scaffolds exhibited more extensive cell spreading over the fibrous network. Consistent with these observations, the MTT results showed increasing metabolic activity from day 1 to day 7 in all scaffold groups. The higher metabolic activity observed on the crosslinked pVEGF polyplex-loaded scaffolds at later time points may be related to the improved structural stability of the crosslinked fibrous network, which preserved the scaffold architecture during culture and provided a more stable substrate for cell attachment and growth. In addition, sustained VEGF expression from the pVEGF polyplex-loaded scaffolds may have contributed to the enhanced HUVEC response. Overall, these findings indicate that genipin crosslinking did not compromise scaffold cytocompatibility and that the developed core–shell fibrous scaffolds supported HUVEC attachment and continued metabolic activity during the evaluated culture period. Although endothelial cell migration was not directly assessed in the present study, the VEGF ELISA results provided quantitative evidence of prolonged VEGF secretion following scaffold-mediated pVEGF polyplex delivery. Because VEGF is closely associated with endothelial angiogenic responses, future studies should include direct migration assays, such as scratch-wound or transwell migration assays, to determine whether the released pVEGF polyplexes enhance endothelial cell migration.

The release profile is a key objective in designing controlled-release systems, because it determines whether the therapeutic cargo remains locally available over a prolonged period. In the present study, all core–shell scaffolds exhibited an initial release phase followed by a slower, sustained-release period. This behavior is consistent with the reservoir function of the core–shell architecture, in which the surrounding gelatin/PCL shell acts as a diffusion barrier and delays transport of the encapsulated cargo from the aqueous core into the release medium [76]. Biomolecule release from biodegradable polymeric scaffolds may be governed by diffusion through interconnected pores, polymer swelling and relaxation, matrix dissolution or degradation, and interactions between the cargo and polymeric matrix [77]. In the present system, the marked reduction in the early release of polyplexes after genipin treatment indicates that crosslinking reduced the permeability of the gelatin-containing shell and restricted diffusion during the initial release period, whereas subsequent stages are primarily controlled by the degradation of the polymeric shell [78].

The release behavior also depended strongly on the physicochemical characteristics of the encapsulated cargo. From crosslinked webs, BSA release reached 54.96% within the first 3 h and 93.34% after 33 d, whereas the cumulative release of polyplexes reached only 25.50% and 57.38% at the same time points. Thus, the initial release of polyplexes was approximately 54% lower than that of BSA. This slower release is likely related to the larger hydrodynamic size and more complex structure of the $bPEI_{1.8}$-DA/pVEGF polyplexes compared with the soluble BSA molecule. BSA can diffuse relatively rapidly through hydrated pores because of its high aqueous solubility, whereas nanoscale polyplexes experience greater steric resistance while traversing the shell matrix. In addition, physical and electrostatic interactions between the cationic polyplexes and the gelatin/PCL-containing shell may further retard their diffusion [19, 79]. The greater effect of crosslinking on polyplex release than on BSA release suggests that transport of the larger nanocomplexes was more sensitive to changes in shell density and pore accessibility.

The thread configuration further reduced the release rate compared with the corresponding web architecture. The initial release of polyplexes from crosslinked threads was 16.59%, approximately 35% lower than that from crosslinked webs, and cumulative release remained lower throughout the 33 d period. Threads made from the core-shell fibers did not significantly affect the release profiles, but decreased the overall release rate. A similar architecture-dependent trend was observed for BSA, confirming that the reduction was not limited to the polyplex cargo. Twisting aligned fibers into a cohesive thread produces a denser fiber arrangement, reduces the effective surface area directly exposed to the medium, and may decrease inter-fiber pore size while increasing the diffusion path length [80, 81]. These structural features provide a plausible explanation for the lower burst release and slower cumulative release observed from the thread configuration.

Overall, the crosslinked core–shell threads released $bPEI_{1.8}$-DA/pVEGF polyplexes gradually over 33 d, with a modest initial release followed by prolonged delivery. Such a profile is desirable for VEGF gene delivery because it may provide an initial amount of polyplexes for early cellular transfection while maintaining polyplex availability during the subsequent culture period. The delayed and sustained VEGF secretion measured by ELISA, particularly the later secretion maximum and higher VEGF levels at days 21 and 28 in the thread group, was consistent with the slower polyplex release observed from this architecture. Nevertheless, the ability of this release profile to promote mature and functional blood vessel formation requires confirmation using direct migration, angiogenesis, and *in vivo* vascularization studies.

The fluorescence-based release study confirmed the sustained release of FITC-labeled polyplex-associated components from the core–shell fibrous scaffolds. However, fluorescence-based release alone does not directly demonstrate whether the released polyplexes retain their gene expression capability or biological activity. Therefore, complementary functional assays were performed using pEGFP as a reporter plasmid and ELISA to quantify

VEGF secretion. The observation of EGFP-positive HUVECs after exposure to bPEI$_{1.8}$-DA/pEGFP polyplexes released from the scaffolds indicated that the polyplexes retained the ability to mediate reporter-gene expression after electrospinning, scaffold incorporation, and release. This finding is particularly relevant because exposure to the electrospinning environment, organic solvents in the shell phase, aqueous incubation conditions, and interactions with the polymeric matrix could potentially affect polyplex stability and transfection performance.

The ELISA results provided functional evidence that the released pVEGF polyplexes were able to induce VEGF protein secretion by HUVECs. While the release study confirmed the sustained release of polyplexes from the core–shell scaffolds, ELISA further demonstrated that the released polyplexes retained biological activity and supported VEGF production at the cellular level. Free bPEI$_{1.8}$-DA/pVEGF polyplexes produced an early VEGF secretion maximum followed by a marked decline, consistent with their immediate availability to HUVECs and the limited duration of a single free-polyplex exposure. The web group reached its maximum VEGF concentration at day 7, whereas the thread group reached its maximum at day 14 and maintained significantly higher VEGF concentrations than the web group at days 21 and 28. These temporal differences were consistent with the corresponding release profiles and indicate that scaffold architecture influenced the duration of polyplex availability and downstream VEGF production. The more prolonged VEGF secretion observed for the thread group can be related to its compact fibrous architecture. Twisting aligned fibers into a cohesive thread likely reduced the effective surface area exposed to the culture medium, decreased inter-fiber pore accessibility, and increased the diffusion path length compared with the nonwoven web. These structural characteristics reduced the initial release and prolonged polyplex availability, which was reflected in the delayed VEGF secretion profile. Therefore, the thread configuration not only controlled polyplex release but also prolonged the downstream VEGF protein secretion by HUVECs. Overall, the ELISA findings support the suitability of the core–shell fibrous thread as a sustained gene delivery platform capable of extending VEGF protein secretion over time. These results strengthen the rationale for using pVEGF polyplex-loaded fibrous threads as threshold-guided angiogenic constructs for future vascularization strategies.

To further explain how the released polyplexes may mediate gene expression in HUVECs, the cellular entry mechanism should be considered. The released plasmid is expected to be delivered to HUVECs in the form of bPEI$_{1.8}$-DA/plasmid polyplexes rather than as naked plasmid DNA. The cationic nature of bPEI$_{1.8}$-DA enables condensation of plasmid DNA into nanoscale polyplexes and can promote interaction with the negatively charged cell membrane. In addition, deoxycholic acid modification may enhance membrane interaction due to its amphiphilic character. Based on previous mechanistic studies on bPEI$_{1.8}$-DA conjugates, cellular uptake of these polyplexes is mainly associated with endocytic internalization followed by intracellular release of the nucleic acid cargo [62]. In the present study, EGFP expression and VEGF secretion provide functional evidence that the released polyplexes mediated intracellular gene expression. However, direct mechanistic studies such as uptake inhibition, endosomal co-localization, or intracellular trafficking analysis were not performed in the present work and should be included in future studies to further clarify the cellular entry pathway of the released polyplexes.

As discussed above, the local level and duration of VEGF exposure are critical determinants of angiogenic outcome. Although VEGF is a potent regulator of endothelial activation and vessel formation, excessive or poorly controlled VEGF expression can lead to abnormal, immature, and leaky vascular structures. Previous studies have suggested that maintaining VEGF expression below a critical microenvironmental threshold may promote more organized angiogenesis, whereas excessive VEGF levels may shift the response toward aberrant vascular growth or hemangioma-like structures [14, 16]. Ozawa *et al* proposed that VEGF production in the range of approximately 70–100 ng 10^{-6} cells/day represents a boundary between controlled angiogenesis and hemangioma-like vascular responses [16]. Therefore, delivery systems designed for VEGF-based angiogenic stimulation should ideally provide localized and sustained VEGF availability while avoiding excessive early exposure. For a gene-delivering scaffold, a desirable release profile would include a moderate initial release to make the gene vector available for early cellular transfection, followed by a slower and sustained release phase to maintain local transgene expression over an extended period [82].

In the present study, the core–shell architecture and genipin crosslinking reduced the burst release of bPEI$_{1.8}$-DA/pVEGF polyplexes, while the compact thread configuration further slowed cumulative release compared with the web configuration. The initial release of polyplexes was 25.50% from crosslinked webs and 16.59% from crosslinked threads, and the thread configuration maintained a lower cumulative released amount throughout the 33 d period. When the cumulative release was expressed in ng, the thread configuration maintained the released polyplex amount below the 100 ng reference level for up to 16 d and reached approximately 106 ng by day 22. This result indicates that the thread architecture more closely approached the intended low-release profile than the corresponding web scaffold. The biological relevance of this release behavior was supported by the VEGF ELISA results,

where the thread group showed a delayed secretion maximum at day 14 and maintained higher VEGF levels than the web group at later time points. However, this value should be interpreted as a comparative reference rather than a direct VEGF biological threshold, because the previously reported threshold refers to VEGF protein production under specific cellular conditions, whereas the present data represent released pVEGF polyplexes. The critical level must be determined relative to the specific application, the target environment, and the local concentration of GFs. The present findings suggest that the core–shell fibrous thread can extend pVEGF polyplex availability and prolong downstream VEGF secretion. Nevertheless, direct angiogenic outcomes, including endothelial migration, tube formation, vessel maturation, and *in vivo* vascularization, should be evaluated in future studies.

5. Conclusion

In this study, aligned core–shell fibrous threads loaded with bPEI$_{1.8}$-DA/pVEGF polyplexes were successfully developed as a scaffold-mediated platform for sustained VEGF gene delivery. The gelatin/PCL (70:30) shell and aqueous polyplex-containing core were fabricated using a modified coaxial electrospinning system equipped with a rotating disk collector. SEM, FM, and TEM analyses confirmed the formation of bead-free aligned fibers with a core–shell architecture and successful incorporation of polyplexes within the fibrous structures. Genipin crosslinking preserved the fibrous morphology and improved scaffold stability, while modifying the mechanical response of the threads by increasing Young's modulus and reducing extensibility. The *in vitro* release results demonstrated that the core–shell architecture, genipin crosslinking, and compact thread configuration collectively reduced the initial burst release and prolonged the delivery of bPEI$_{1.8}$-DA/pVEGF polyplexes over 33 d. Compared with the corresponding web scaffold, the crosslinked thread configuration reduced the initial release by approximately 34%, and the released polyplex amount remained below the 100 ng reference level for up to 16 d. This indicates that the aligned and compact fibrous arrangement provided an additional barrier to diffusion. The released polyplexes retained functional gene expression capability, as shown by EGFP reporter-gene expression in HUVECs after exposure to scaffold-released pEGFP polyplexes. In addition, VEGF ELISA confirmed that scaffold-mediated delivery of bPEI$_{1.8}$-DA/pVEGF polyplexes induced VEGF secretion by HUVECs. The thread group exhibited a delayed VEGF secretion maximum and maintained higher VEGF levels at later time points compared with the web group, consistent with its slower polyplex release profile.

The developed scaffolds also supported HUVEC adhesion and metabolic activity, indicating that the crosslinked gelatin/PCL core–shell fibrous platform was cytocompatible under the evaluated *in vitro* conditions. Overall, these findings demonstrate that core–shell fibrous threads can provide sustained pVEGF polyplex availability, prolong downstream VEGF secretion, and maintain scaffold cytocompatibility and structural integrity. This thread-based platform may therefore be useful for future angiogenesis-oriented tissue-engineering strategies, particularly in applications where directional fibrous architecture and localized gene-vector delivery are required. Further studies evaluating endothelial migration, tube formation, vessel maturation, and *in vivo* vascularization are required to confirm the biological effectiveness and safety of this system.

Acknowledgment

The authors express their gratitude to the National Cell Bank of the Pasteur Institute of Iran for providing technical expertise regarding the cell culture experiments. Furthermore, appreciation is extended to the Department of Cell Engineering at the Royan Institute's Cell Science Research Center in Iran for their vital contributions toward material synthesis and the provision of essential reagents.

Data availability statement

The data cannot be made publicly available upon publication because they are not available in a format that is sufficiently accessible or reusable by other researchers. The data that support the findings of this study are available upon reasonable request from the authors.

ORCID iD

Farzaneh Ghasemkhah 0009-0002-0034-9141

References

[1] Chapekar M S 2000 Tissue engineering: challenges and opportunities *J. Biomed. Mater. Res.* **53** 617–20
[2] Jain R K, Au P, Tam J, Duda D G and Fukumura D 2005 Engineering vascularized tissue *Nat. Biotechnol.* **23** 821–3
[3] Novosel E C, Kleinhans C and Kluger P J 2011 Vascularization is the key challenge in tissue engineering *Adv. Drug. Deliv. Rev.* **63** 300–11
[4] Hadjizadeh A and Doillon C J 2010 Directional migration of endothelial cells towards angiogenesis using polymer fibres in a 3D co-culture system *J. Tissue Eng. Regen. Med.* **4** 524–31
[5] Xiao Y *et al* 2026 Preparation and *in vivo* effectiveness evaluation of heparin-loaded PLGA@ PCL core-shell fiber small-diameter vascular grafts *PLoS One* **21** e0337192
[6] Sahoo S, Ang L T, Goh J C-H and Toh S-L 2010 Growth factor delivery through electrospun nanofibers in scaffolds

for tissue engineering applications *J. Biomed. Mater. Res. A* **93** 1539–50
[7] Pajooh A M D *et al* 2024 Biomimetic VEGF-loaded bilayer scaffold fabricated by 3D printing and electrospinning techniques for skin regeneration *Mater. Des.* **238** 112714
[8] Ku S H and Park C B 2010 Human endothelial cell growth on mussel-inspired nanofiber scaffold for vascular tissue engineering *Biomaterials* **31** 9431–7
[9] Gounis M, Spiga M-G, Graham R M, Wilson A, Haliko S, Lieber B B, Wakhloo A K and Webster K A 2005 Angiogenesis is confined to the transient period of VEGF expression that follows adenoviral gene delivery to ischemic muscle *Gene Ther.* **12** 762–71
[10] DeVolder R J, Bae H, Lee J and Kong H 2011 Directed blood vessel growth using an angiogenic microfiber/microparticle composite patch *Adv. Mater.* **23** 3139–43
[11] Cojocaru E, Ghitman J and Stan R 2022 Electrospun-fibrous-architecture-mediated non-viral gene therapy drug delivery in regenerative medicine *Polymers* **14** 2647
[12] Al Fahad M A, Lee H-Y, Park S, Choi M, Shanto P C, Park M, Bae S H and Lee B-T 2024 Small-diameter vascular graft composing of core-shell structured micro-nanofibers loaded with heparin and VEGF for endothelialization and prevention of neointimal hyperplasia *Biomaterials* **306** 122507
[13] Sun Y, Heacock J, Liu J and Li Y V 2025 Enhanced fibrous scaffolds for drug delivery applications: core–shell fiber scaffolds with antibiotic-encapsulated poly (lactic-co-glycolic acid) nanoparticles *ACS Appl. Nano Mater.* **8** 5853–61
[14] Banfi A, von Degenfeld G and Blau H M 2005 Critical role of microenvironmental factors in angiogenesis *Curr. Atheroscler. Rep.* **7** 227–34
[15] Hoeben A, Landuyt B, Highley M S, Wildiers H, Van Oosterom A T and De Bruijn E A 2004 Vascular endothelial growth factor and angiogenesis *Pharmacol. Rev.* **56** 549–80
[16] Ozawa C R, Banfi A, Glazer N L, Thurston G, Springer M L, Kraft P E, McDonald D M and Blau H M 2004 Microenvironmental VEGF concentration, not total dose, determines a threshold between normal and aberrant angiogenesis *J. Clin. Invest.* **113** 516–27
[17] Zacchigna S *et al* 2007 vivo imaging shows abnormal function of vascular endothelial growth factor-induced vasculature *Hum. Gene Ther.* **18** 515–24
[18] Liu Y, Yuan H, Liu Y, Chen C, Tang Z, Huang C, Ning Z, Lu T and Wu Z 2023 Multifunctional nanoparticle-VEGF modification for tissue-engineered vascular graft to promote sustained anti-thrombosis and rapid endothelialization *Front. Bioeng. Biotechnol.* **11** 1109058
[19] He S, Xia T, Wang H, Wei L, Luo X and Li X 2012 Multiple release of polyplexes of plasmids VEGF and bFGF from electrospun fibrous scaffolds towards regeneration of mature blood vessels *Acta Biomater.* **8** 2659–69
[20] Zhang H, Jia X, Han F, Zhao J, Zhao Y, Fan Y and Yuan X 2013 Dual-delivery of VEGF and PDGF by double-layered electrospun membranes for blood vessel regeneration *Biomaterials* **34** 2202–12
[21] An J, Li S, Ma T, Chen Y, Santerre J P, Wang W and Zhang X 2026 Co-delivery of endometrial mesenchymal stem cells and macrophages by an electrospun patch promotes angiogenesis during endometrial injury repair via VEGF related signalling *Stem Cell Res. Ther.* **17** 108
[22] Tessmar J K and Göpferich A M 2007 Matrices and scaffolds for protein delivery in tissue engineering *Adv. Drug. Deliv. Rev.* **59** 274–91
[23] Porter J R, Ruckh T T and Popat K C 2009 Bone tissue engineering: a review in bone biomimetics and drug delivery strategies *Biotechnol. Prog.* **25** 1539–60
[24] Hadjiargyrou M and Chiu J B 2008 Enhanced composite electrospun nanofiber scaffolds for use in drug delivery *Expert Opin. Drug Deliv.* **5** 1093–106
[25] Hadjizadeh A, Ghasemkhah F and Ghasemzaie N 2017 Polymeric scaffold based gene delivery strategies to improve angiogenesis in tissue engineering: a review *Polym. Rev.* **57** 505–56
[26] Ylä-herttuala S, Bridges C, Katz M G and Korpisalo P 2017 Angiogenic gene therapy in cardiovascular diseases: dream or vision? *Eur. Heart J.* **38** 1365–71
[27] Pan P, Li J, Liu X, Hu C, Wang M, Zhang W, Li M and Liu Y 2023 Plasmid containing VEGF-165 and ANG-1 dual genes packaged with fibroin-modified PEI to promote the regeneration of vascular network and dermal tissue *Colloids Surf. B* **224** 113210
[28] Tsurumi Y, Takeshita S, Chen D, Kearney M, Rossow S T, Passeri J, Horowitz J R, Symes J F and Isner J M 1996 Direct intramuscular gene transfer of naked DNA encoding vascular endothelial growth factor augments collateral development and tissue perfusion *Circulation* **94** 3281–90
[29] Kalka C *et al* 2000 Vascular endothelial growth factor165 gene transfer augments circulating endothelial progenitor cells in human subjects *Circ. Res.* **86** 1198–202
[30] Rabinovsky E D and Draghia-akli R 2004 Insulin-like growth factor I plasmid therapy promotes *in vivo* angiogenesis *Mol. Ther.* **9** 46–55
[31] Godbey W, Wu K K and Mikos A G 1999 Poly (ethylenimine) and its role in gene delivery *J. Control. Release* **60** 149–60
[32] Akinc A, Thomas M, Klibanov A M and Langer R 2005 Exploring polyethylenimine-mediated DNA transfection and the proton sponge hypothesis *J. Gene Med.* **7** 657–63
[33] Pack D W, Hoffman A S, Pun S and Stayton P S 2005 Design and development of polymers for gene delivery *Nat. Rev. Drug Discov.* **4** 581–93
[34] Lungwitz U, Breunig M, Blunk T and Göpferich A 2005 Polyethylenimine-based non-viral gene delivery systems *Eur. J. Pharm. Biopharm.* **60** 247–66
[35] Dai J, Zou S, Pei Y, Cheng D, Ai H and Shuai X 2011 Polyethylenimine-grafted copolymer of poly (l-lysine) and poly (ethylene glycol) for gene delivery *Biomaterials* **32** 1694–705
[36] Jiang D and Salem A K 2012 Optimized dextran–polyethylenimine conjugates are efficient non-viral vectors with reduced cytotoxicity when used in serum containing environments *Int. J. Pharm.* **427** 71–79
[37] Kichler A 2004 Gene transfer with modified polyethylenimines *J. Gene Med.* **6** S3–S10
[38] Wang X *et al* 2010 Synthesis and evaluation of chitosan-graft-polyethylenimine as a gene vector *Die Pharmazie.* **65** 572–9 (In German)
[39] Wang H-Y, Sun Y-X, Deng J-Z, Yang J, Zhuo R-X and Zhang X-Z 2012 Effect of peptides and their introduction methods on target gene transfer of gene vector based on disulfide-containing polyethyleneimine *Int. J. Pharm.* **438** 191–201
[40] Jeon O, Yang H S, Lee T-J and Kim B-S 2008 Heparin-conjugated polyethylenimine for gene delivery *J. Control. Release* **132** 236–42
[41] Sawant R R, Sriraman S K, Navarro G, Biswas S, Dalvi R A and Torchilin V P 2012 Polyethyleneimine-lipid conjugate-based pH-sensitive micellar carrier for gene delivery *Biomaterials* **33** 3942–51
[42] Kim D, Ku S H, Kim H, Jeong J H, Lee M, Kwon I C, Choi D and Kim S H 2016 Simultaneous regulation of apoptotic gene silencing and angiogenic gene expression for myocardial infarction therapy: single-carrier delivery of SHP-1 siRNA and VEGF-expressing pDNA *J. Control. Release* **243** 182–94
[43] Amjad M W, Amin M C I M, Katas H, Butt A M, Kesharwani P and Iyer A K 2015 In vivo antitumor activity of folate-conjugated cholic acid-polyethylenimine micelles for the codelivery of doxorubicin and siRNA to colorectal adenocarcinomas *Mol. Pharm.* **12** 4247–58
[44] MoonHH J 2014 MSC-based VEGF gene therapy in rat myocardial infarction model using facial amphipathic bile acid-conjugated polyethyleneimine *Biomaterials* **35** 1744–54
[45] Kish P E, Tsume Y, Kijek P, Lanigan T M, Hilfinger J M and Roessler B J 2007 Bile acid—oligopeptide conjugates interact with DNA and facilitate transfection *Mol. Pharm.* **4** 95–103

[46] Kim D, Lee D, Jang Y L, Chae S Y, Choi D, Jeong J H and Kim S H 2012 Facial amphipathic deoxycholic acid-modified polyethyleneimine for efficient MMP-2 siRNA delivery in vascular smooth muscle cells *Eur. J. Pharm. Biopharm.* **81** 14–23
[47] Jang J-H, Houchin T L and Shea L D 2004 Gene delivery from polymer scaffolds for tissue engineering *Expert Rev. Med. Devices* **1** 127–38
[48] Ochiya T, Nagahara S, Sano A, Itoh H and Terada M 2001 Biomaterials for gene delivery atelocollagen-mediated controlled release of molecular medicines *Curr. Gene Ther.* **1** 31–52
[49] Chen F, Wan H, Xia T, Guo X, Wang H, Liu Y and Li X 2013 Promoted regeneration of mature blood vessels by electrospun fibers with loaded multiple pDNA-calcium phosphate nanoparticles *Eur. J. Pharm. Biopharm.* **85** 699–710
[50] Wang X, Ding B and Li B 2013 Biomimetic electrospun nanofibrous structures for tissue engineering *Mater. Today* **16** 229–41
[51] Zamani F *et al* 2017 Nanofibrous and nanoparticle materials as drug-delivery systems *Nanostructures for Drug Delivery* (Elsevier) pp 239–70
[52] Tian Z, Zhao Z, Rausch M A, Behm C, Tur D, Shokoohi-tabrizi H A, Andrukhov O and Rausch-fan X 2025 Potential of trilayered gelatin/polycaprolactone nanofibers for periodontal regeneration: an in vitro study *Int. J. Mol. Sci.* **26** 672
[53] Ji W, Sun Y, Yang F, van den Beucken J J J P, Fan M, Chen Z and Jansen J A 2011 Bioactive electrospun scaffolds delivering growth factors and genes for tissue engineering applications *Pharm. Res.* **28** 1259–72
[54] Liao I-C, Chen S, Liu J B and Leong K W 2009 Sustained viral gene delivery through core-shell fibers *J. Control. Release* **139** 48–55
[55] Saraf A, Baggett L S, Raphael R M, Kasper F K and Mikos A G 2010 Regulated non-viral gene delivery from coaxial electrospun fiber mesh scaffolds *J. Control. Release* **143** 95–103
[56] Alizadeh S, Samadikuchaksaraei A, Jafari D, Orive G, Dolatshahi-pirouz A, Pezeshki-modaress M and Gholipourmalekabadi M 2024 Enhancing diabetic wound healing through improved angiogenesis: the role of emulsion-based core-shell micro/nanofibrous scaffold with sustained CuO nanoparticle delivery *Small* **20** 2309164
[57] Wang B, Lu G, Song K, Chen A, Xing H, Wu J, Sun Q, Li G and Cai M 2023 PLGA-based electrospun nanofibers loaded with dual bioactive agent loaded scaffold as a potential wound dressing material *Colloids Surf. B* **231** 113570
[58] Al Fahad M A, Choi M, Lee H-Y, Shanto P C, Mahbub M S I, Jahan N, Park M, Kim N, Bae S H and Lee B-T 2026 Ex vivo endothelialized cECM-enriched core–shell fibrous vascular graft promotes rapid regenerative remodeling in vivo *Bioact. Mater.* **63** 336–53
[59] Jiang H, Wang L and Zhu K 2014 Coaxial electrospinning for encapsulation and controlled release of fragile water-soluble bioactive agents *J. Control. Release* **193** 296–303
[60] Duan N, Geng X, Ye L, Zhang A, Feng Z, Guo L and Gu Y 2016 A vascular tissue engineering scaffold with core–shell structured nano-fibers formed by coaxial electrospinning and its biocompatibility evaluation *Biomed. Mater.* **11** 035007
[61] Ghasemkhah F, Latifi M, Hadjizadeh A and Shokrgozar M A 2019 Potential core–shell designed scaffolds with a gelatin-based shell in achieving controllable release rates of proteins for tissue engineering approaches *J. Biomed. Mater. Res. A* **107** 1393–405
[62] Radmanesh F, Abandansari H S, Pahlavan S, Alikhani M, Karimi M, Rajabi S, Kazemi B and Baharvand H 2019 Optimization of miRNA delivery by using a polymeric conjugate based on deoxycholic acid-modified polyethylenimine *Int. J. Pharm.* **565** 391–408
[63] Panzavolta S, Gioffrè M, Focarete M L, Gualandi C, Foroni L and Bigi A 2011 Electrospun gelatin nanofibers: Optimization of genipin cross-linking to preserve fiber morphology after exposure to water *Acta Biomaterialia* **7** 1702–9
[64] Gautam S, Dinda A K and Mishra N C 2013 Fabrication and characterization of PCL/gelatin composite nanofibrous scaffold for tissue engineering applications by electrospinning method *Mater. Sci. Eng. C* **33** 1228–35
[65] Ghasemi-mobarakeh L, Prabhakaran M P, Morshed M, Nasr-esfahani M-H and Ramakrishna S 2008 Electrospun poly (ε-caprolactone)/gelatin nanofibrous scaffolds for nerve tissue engineering *Biomaterials* **29** 4532–9
[66] Kim M S, Jun I, Shin Y M, Jang W, Kim S I and Shin H 2010 The development of genipin-crosslinked poly (caprolactone)(PCL)/gelatin nanofibers for tissue engineering applications *Macromol. Biosci.* **10** 91–100
[67] Li Q, Wang X, Lou X, Yuan H, Tu H, Li B and Zhang Y 2015 Genipin-crosslinked electrospun chitosan nanofibers: determination of crosslinking conditions and evaluation of cytocompatibility *Carbohydrate Polym.* **130** 166–74
[68] Del Gaudio C, Baiguera S, Boieri M, Mazzanti B, Ribatti D, Bianco A and Macchiarini P 2013 Induction of angiogenesis using VEGF releasing genipin-crosslinked electrospun gelatin mats *Biomaterials* **34** 7754–65
[69] Mintzer M A and Simanek E E 2009 Nonviral vectors for gene delivery *Chem. Rev.* **109** 259–302
[70] Wong S Y, Pelet J M and Putnam D 2007 Polymer systems for gene delivery—past, present, and future *Prog. Polym. Sci.* **32** 799–837
[71] Poursamar S A, Lehner A N, Azami M, Ebrahimi-barough S, Samadikuchaksaraei A and Antunes A P M 2016 The effects of crosslinkers on physical, mechanical, and cytotoxic properties of gelatin sponge prepared via *in-situ* gas foaming method as a tissue engineering scaffold *Mater. Sci. Eng. C* **63** 1–9
[72] Chou S-F, Luo L-J, Lai J-Y and Ma D H-K 2017 Role of solvent-mediated carbodiimide cross-linking in fabrication of electrospun gelatin nanofibrous membranes as ophthalmic biomaterials *Mater. Sci. Eng. C* **71** 1145–55
[73] Lim C, Tan E and Ng S 2008 Effects of crystalline morphology on the tensile properties of electrospun polymer nanofibers *Appl. Phys. Lett.* **92** 141908
[74] Kołbuk D, Sajkiewicz P, Maniura-weber K and Fortunato G 2013 Structure and morphology of electrospun polycaprolactone/gelatine nanofibres *Eur. Polym. J.* **49** 2052–61
[75] Baji A, Mai Y-W, Wong S-C, Abtahi M and Chen P 2010 Electrospinning of polymer nanofibers: effects on oriented morphology, structures and tensile properties *Compos. Sci. Technol.* **70** 703–18
[76] Puppi D and Chiellini F 2018 Drug release kinetics of electrospun fibrous systems *Core-shell Nanostructures for Drug Delivery and Theranostics* (Elsevier) pp 349–74
[77] Buzgo M *et al* 2018 Blend electrospinning, coaxial electrospinning, and emulsion electrospinning techniques *Core-shell Nanostructures for Drug Delivery and Theranostics* (Elsevier) pp 325–47
[78] Ji W, Yang F, van den Beucken J J J P, Bian Z, Fan M, Chen Z and Jansen J A 2010 Fibrous scaffolds loaded with protein prepared by blend or coaxial electrospinning *Acta Biomater.* **6** 4199–207
[79] Yang Y, Li X, Cheng L, He S, Zou J, Chen F and Zhang Z 2011 Core–sheath structured fibers with pDNA polyplex loadings for the optimal release profile and transfection efficiency as potential tissue engineering scaffolds *Acta Biomater.* **7** 2533–43
[80] He C L, Huang Z M and Han X J 2009 Fabrication of drug-loaded electrospun aligned fibrous threads for suture applications *J. Biomed. Mater. Res. A* **89** 80–95
[81] Maleki H, Gharehaghaji A A, Toliyat T and Dijkstra P J 2016 Drug release behavior of electrospun twisted yarns as implantable medical devices *Biofabrication* **8** 035019
[82] Zigdon-giladi H, Khutaba A, Elimelech R, Machtei E E and Srouji S 2017 VEGF release from a polymeric nanofiber scaffold for improved angiogenesis *J. Biomed. Mater. Res. A* **105** 2712–21